1·0

2·8   2·5

3·15   2·2

3·5

1·1   4·0   2·0

1·8

1·25   1·4   1·6

NATIONAL BUREAU OF STANDARDS
MICROCOPY RESOLUTION TEST CHART

LEVEL

Forced Response of a Blasius Flat-Plate Boundary Layer to an External Vortex Street

J. W. ELLINWOOD
Laboratory Operations
The Aerospace Corporation
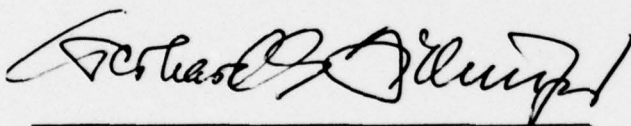El Segundo, Calif. 90245

5 July 1979

79 08 7 004

Prepared for

SPACE AND MISSILE SYSTEMS ORGANIZATION
AIR FORCE SYSTEMS COMMAND
Los Angeles Air Force Station
P.O. Box 92960, Worldway Postal Center
Los Angeles, Calif. 90009

Gerhard E. Aichinger
Project Officer

FOR THE COMMANDER

Frank J. Bane, Chief
Contracts Management Office

REPORT DOCUMENTATION PAGE		READ INSTRUCTIONS BEFORE COMPLETING FORM
1. REPORT NUMBER SAMSO-TR-79-65	2. GOVT ACCESSION NO.	3. RECIPIENT'S CATALOG NUMBER
4. TITLE *(and Subtitle)* Forced Response of a Blasius Flat-Plate Boundary Layer to an External Vortex Street		5. TYPE OF REPORT & PERIOD COVERED Interim rept.
		6. PERFORMING ORG. REPORT NUMBER TR-0079(4940-01)-5
7. AUTHOR(s) J. W. Ellinwood		8. CONTRACT OR GRANT NUMBER(s) F04701-78-C-0079
9. PERFORMING ORGANIZATION NAME AND ADDRESS The Aerospace Corporation El Segundo, California 90245		10. PROGRAM ELEMENT, PROJECT, TASK AREA & WORK UNIT NUMBERS
11. CONTROLLING OFFICE NAME AND ADDRESS Space and Missile Systems Organization Air Force Systems Command Los Angeles, Calif. 90009		12. REPORT DATE 5 July 1979
		13. NUMBER OF PAGES 66
14. MONITORING AGENCY NAME & ADDRESS(*If different from Controlling Office*)		15. SECURITY CLASS. (*of this report*) Unclassified
		15a. DECLASSIFICATION/DOWNGRADING SCHEDULE

16. DISTRIBUTION STATEMENT (*of this Report*)

Approved for public release; distribution unlimited.

17. DISTRIBUTION STATEMENT (*of the abstract entered in Block 20, if different from Report*)

18. SUPPLEMENTARY NOTES

19. KEY WORDS (*Continue on reverse side if necessary and identify by block number*)

Fluid dynamics
Boundary layer stability and transition
Tollmien-Schlichting wave

20. ABSTRACT (*Continue on reverse side if necessary and identify by block number*)

An asymptotic theory is presented for two-dimensional disturbances in the wake of an oscillating shedding-vortex line source and in the local presence of a semi-infinite flat plate and its boundary layer. No instabilities were sought or excited. The very large parameter is a Reynolds number; the shedding frequency is moderate. The boundary layer is comprised of three sublayers. In the outer "edge" sublayer, where the Blasius variable is logarithmically large, the disturbance velocities are described analytically by Kelvin functions.

DD FORM 1473
(FACSIMILE)

Results compare qualitatively with previous numerical and experimental findings and indicate that the boundary layer effectively suppresses the external disturbances. Those disturbances that remain in the boundary layer peak at a finite (large) Reynolds number and finite frequency.

PREFACE

1

CONTENTS

3

FIGURES

PAGES 2 & 4 BLANK

1. Introduction

It has been observed experimentally (Schubauer and Skramstad 1948; Ross et al. 1970) that the earliest stage of boundary-layer transition on smooth flat plates in low-turbulence streams involves the rapid growth of two-dimensional traveling waves known as Tollmien-Schlichting waves. With the boundary-layer stability theory, only the growth rate of these plane waves can be estimated satisfactorily. The necessary link between the initial amplitude of these waves and the ambient disturbance level is as unknown today as it was 30 years ago (Mack 1977). Tollmien-Schlichting waves can most certainly be excitable analytically. The nature of their excitation has not yet been defined but must require, as does the excitation of any resonant oscillation, superposition of complementary solutions (conceptually provided by stability theory) and of particular solutions for boundary-layer response to local external disturbances. Treatments of the latter are incomplete, and more research, such as the present theory, is needed (Reshotko 1976; Arnal and Juillen 1977).

There are three theories to explain unsteady infinitesimal disturbances in a laminar boundary layer. In one, it is assumed that the surface is vibrated in the streamwise direction, producing uniform oscillatory ambient flow (Riley 1975; Patel 1973). In another, the effect of sound on laminar boundary layers (Illingworth 1958; Mack 1975) is studied, a coupling that is fairly well understood but has little effect in subsonic wind tunnels (Reshotko 1976). In a third and in the present study, the effects of ambient

7

convected disturbances are investigated. In these models, the freestream turbulence or vorticity, the most influential triggers of transition in low-speed wind tunnels, are approximated. Kestin, Meader, and Wang (1961) assumed that the waves were oriented to travel purely in the streamwise direction. They calculated the first departure from a quasi-steady flow. Criminale (1976, 1971) assumed that the frequency and all wavenumbers were real and found the effect of a point source of normal velocity located at the finite boundary layer edge. He concluded erroneously that the largest disturbances occur in the boundary layer. Rogler and Reshotko (1975) investigated a model in which the imposed convected disturbances form a square vortex lattice that did not decay downstream. Their study, as does this, indicates that maximum disturbance velocity occurs outside the boundary layer and that maximum disturbance vorticity occurs at the surface.

The present theory advances the field in several ways. Because it is an asymptotic theory for very large Reynolds numbers, closed-form expressions for maximal disturbance velocities are achieved, as well as explicit parameter variations not given by numerical calculations at a finite Reynolds number. The present formulae alone are simple enough that they can be combined later with complementary solutions from asymptotic stability theory to explain how convected disturbances generate Tollmien-Schlichting waves. A fundamental solution (for a harmonic line source at a generic location upstream) is presented, thus allowing the description of

8

particular disturbance fields such as the square lattice of Rogler and Reshotko (1975) by superposition.

Recent studies of the continuous spectrum of the Orr-Sommerfeld equation (Mack 1976; Murdock and Stewartson 1977; Jordinson 1971; Antar and Benek 1978; Grosch and Salwen 1978) allow disturbances of bounded variation far from the surface. These eigenvalue searches are only relevant to descriptions of boundary-layer response, but stability applications were expected. In these studies, a finite boundary-layer thickness was defined and the Reynolds number was finite.

2. Freestream disturbances

A description of the external disturbance field that would exist in the absence of the flat plate helps to explain how the theory for boundary-layer response to a single wavenumber component (Section 3) will be developed into physical variables (Section 4).

Only two-dimensional external disturbances are considered. Since Tollmien-Schlichting waves (of interest for later extension of present theory) are two dimensional, it is unlikely that the spectrum of disturbance energy in the third (transverse) dimension is of critical importance in the initial linear stage of Tollmien-Schlichting wave generation. The spectrum of energy in the normal and streamwise directions _is_ critical for this application, but there is not a standard spectrum in wind tunnels. The present theory can be applied to turbulent streams by integrating the single-frequency theory result over an appropriate spectrum.

In the present theory, the external stream is disturbed only by a single harmonic line disturbance with a laminar wake (figure 1) like a Karman vortex street. Of course, in the usual street scene, the vortices are discrete and have interacted to form a double row. Linearity requires colinear vortices and permits continuous shedding.

There are several reasons why this disturbance was chosen. It is the _most fundamental harmonic_ disturbance from a line source, and any two-dimensional disturbance field can conceptually be generated by use of the present result as a Green's function. This disturbance model closely

11
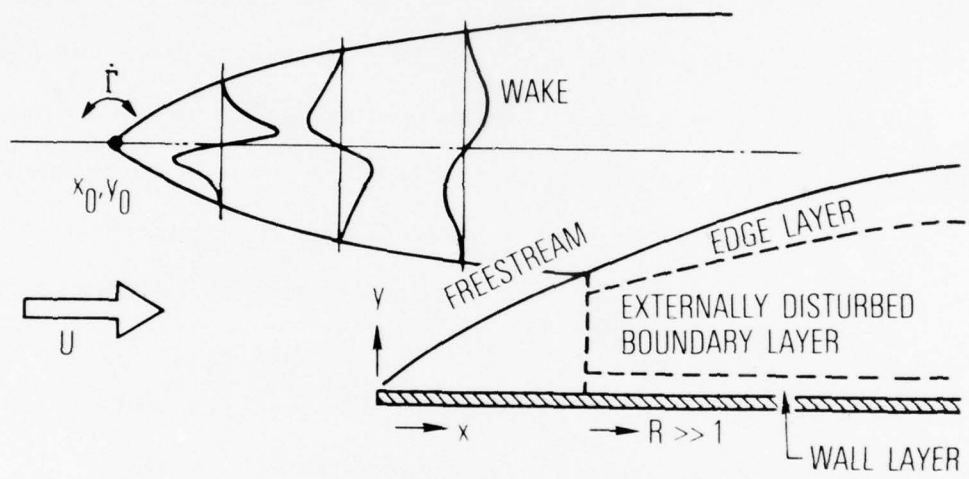
Figure 1. Externally Disturbed Boundary Layer

simulates the effects of the vibrating ribbons used in the critical experiments (Schubauer and Skramstad 1948; Ross et al. 1970; Kachanov, Kozlov, and Levchenko 1976). It enables a physical interpretation of the results (disturbance maxima are presented in Section 4 in physical variables, rather than in wavenumber only). It also provides justification for studying only wavenumbers whose order of magnitude is comparable with reciprocal boundary-layer thickness.

If x denotes the distance downstream from the leading edge, and y the normal distance from the surface, a disturbance stream function ψ provides disturbance velocity components ψ_y and $-\psi_x$. A small cylinder or ribbon (one with a width that is negligible compared to its distance from the leading edge) is located at x_0 and y_0. If at time t_0, the disturbance source sheds a single vortex of circulation Γ, the vortex must consist of both a potential vortex and a rotational core, or the vortex center will not exhibit solid-body rotation (Rott 1964). The rotational core must be convected with the flow in accordance with the vorticity transport equation, and the potential vortex must accompany it, on physical rather than mathematical grounds. The disturbance stream function in the absence of the plate then is

$$\psi(t - t_0) = - \frac{\Gamma}{2\pi} \left\{ \log r + \frac{1}{2} E_1 \left[\frac{r^2}{4\nu(t - t_0)} \right] \right\} \tag{1}$$

where

$$r^2 = \left[x - x_0 - U(t - t_0) \right]^2 + (y - y_0)^2 \tag{2}$$

13

and E_1 denotes the exponential integral. If such vortices are shed continuously and harmonically, beginning at time $t_0 = 0$, with frequency ω and with peak circulation addition rate $\dot{\Gamma}$, then ψ is the real part of

$$\psi = \frac{\dot{\Gamma}}{\Gamma} \int_0^t dt_0 \ e^{-i\omega t_0} \psi(t - t_0) \tag{3}$$

The real part of ψ is assumed throughout. If T is introduced as the time since turnon,

$$e^{i\omega t} \psi = -\frac{\dot{\Gamma}}{4\pi} \int_0^t dT \ e^{i\omega T} \left\{ \log \left[(x - x_0 - UT)^2 + (y - y_0)^2 \right] \right. $$
$$\left. + E_1 \left[\frac{(x - x_0 - UT)^2 + (y - y_0)^2}{4\nu T} \right] \right\} \tag{4}$$

Only the steady-state velocity components are of interest. They are obtained by differentiating ψ with respect to y or x and taking the limit as $t \to \infty$, which exists. When the Reynolds number that is based on the distance downstream from the source $x - x_0$ is very large, the velocity components are explicitly

$$\exp\left[i\omega\left(t - \frac{x - x_0}{U} \right) \right] \begin{Bmatrix} \partial\psi/\partial y \\ \partial\psi/\partial x \end{Bmatrix} = \frac{\dot{\Gamma}}{4U} \begin{Bmatrix} F_+ - F_- \\ i(F_+ + F_-) \end{Bmatrix} \tag{5}$$

where

$$F_{\pm} = \exp\left[\pm\frac{\omega}{U}(y - y_0)\right]\,\mathrm{erfc}\left(\frac{\omega}{U}\left[\frac{\nu(x - x_0)}{U}\right]^{1/2} \pm \frac{(y - y_0)}{2}\left[\frac{U}{\nu(x - x_0)}\right]^{1/2}\right)$$

(6)

The error is of order one over the root Reynolds number. It can be verified that $\partial\psi/\partial y$ is odd in $y - y_0$ and $\partial\psi/\partial x$ is even in $y - y_0$. Both decay transcendentally as the magnitude of $y - y_0$ grows without bound.

It is desired to examine the y-Fourier transform of these components, because the theory for disturbances in the presence of a plate is expressed as the response to a single transverse wavenumber. The velocity transforms are defined by

$$\begin{Bmatrix} \Psi^{(y)} \\ \Psi^{(x)} \end{Bmatrix} = \int_{-\infty}^{\infty} e^{-i\ell y}\exp\left[i\omega\left(t - \frac{x - x_0}{U}\right)\right]\begin{Bmatrix} \partial\psi/\partial y \\ \partial\psi/\partial x \end{Bmatrix}\,dy$$

(7)

and found to be

$$\begin{Bmatrix} \Psi^{(y)} \\ \Psi^{(x)} \end{Bmatrix} = \begin{Bmatrix} \ell \\ \omega/U \end{Bmatrix}\frac{i\dot{\Gamma}}{U}\left(\frac{\omega^2}{U^2} + \ell^2\right)^{-1}\exp\left[-\frac{\nu(x - x_0)}{U}\left(\frac{\omega^2}{U^2} + \ell^2\right) - i\ell y_0\right]$$

(8)

The argument of the exponential function should have a real part of order one if there is to be significant disturbance amplitude. In addition, it is not limiting to assume that $x - x_0$ is comparable with the distance x

15

from the leading edge of a plate, if a plate were present. Therefore,
normalized frequency Ω and transverse wavenumber L are defined as
follows.

$$\frac{\omega x}{U} = \Omega R \qquad \ell x = LR \qquad R = \left(\frac{Ux}{\nu}\right)^{1/2} \qquad (9)$$

The parameters Ω and L are assumed to be of order one. L is real; Ω is
positive. R is the large parameter in this asymptotic theory. In most
stability theories, R is the Reynolds number that is based on some
boundary-layer thickness, but here it is the root x-Reynolds number for
simplicity. With normalized parameters, (8) becomes

$$\begin{Bmatrix} \Psi^{(y)} \\ \Psi^{(x)} \end{Bmatrix} = \begin{Bmatrix} L \\ \Omega \end{Bmatrix} \frac{i\dot{\Gamma}x}{UR(\Omega^2 + L^2)} \exp\left[-\frac{(x - x_0)}{x}(\Omega^2 + L^2) - iL\eta_0\right] \qquad (10)$$

where η_0 is $y_0 R/x$. Thus, the laminar wake behind an oscillating vorticity
source grows parabolically downstream. Its width is of order $x - x_0$ over
the root Reynolds number based on $x - x_0$. This characteristic thickness
establishes the characteristic wavenumber region of interest to be that
where L is of order one. Since the exponential function argument, in square
brackets in (10), has a negative real part of order L^2, no larger $|L|$ than
those of order one need be considered for this type of disturbance source.

Velocity transforms for other line disturbance sources can be found.
For example, if the line source is a symmetric cylinder that oscillates in

16

the streamwise direction, it may develop a periodic drag force by shedding
a vortex <u>doublet</u> sheet. Velocity transforms for such a source also indi-
cate exponential behavior. However, if the line source does <u>not</u> shed any
vorticity, but excites only irrotational disturbances, then these disturbances
die out so fast downstream that they are of no interest. For example, the
stream function for a stationary source-sink oscillator can be found, dif-
ferentiated, and transformed. The y-transforms of the velocity components
are proportional to $\exp\left[-(x-x_0)\,x^{-1}\,|L|R\right]$. This bracketed exponent is a
factor of R more negative than that in (10), where the disturbance is a combi-
nation of rotational and convected potential flow.

In the absence of a plate, the disturbance velocity components are
recovered by taking the inverse transform

$$\exp\left[i\omega\left(t-\frac{x-x_0}{U}\right)\right]\begin{Bmatrix}\partial\psi/\partial y\\\partial\psi/\partial x\end{Bmatrix} = \frac{1}{2\pi}\int_{-\infty}^{\infty}e^{i\ell y}\begin{Bmatrix}\Psi^{(y)}\\\Psi^{(x)}\end{Bmatrix}\,d\ell \qquad (11)$$

In the presence of an aligned semi-infinite flat plate, the disturbance
velocities are more complicated. Additional terms are needed, whose form
in the freestream can be found from the Oseen form of the vorticity trans-
port equation. Thus, outside the plate boundary layer the velocities are
given by

17

$$\exp\left[i\omega\left(t - \frac{x - x_0}{U}\right)\right]\begin{Bmatrix} \partial\psi/\partial y \\ \partial\psi/\partial x \end{Bmatrix} = \frac{1}{2\pi}\int_{-\infty}^{\infty}\left(e^{i\ell y} + C_r^* e^{-i\ell y} + C_w^* e^{-\omega y/U}\right)$$

$$\times \begin{Bmatrix} \Psi^{(y)} \\ \Psi^{(x)} \end{Bmatrix} d\ell \tag{12}$$

where a fourth term, $\propto \exp(\omega y/U)$, has been disallowed on physical grounds. The terms containing C_r^* and C_w^* are for reflected and companion waves, respectively, which are generated by the presence of the no-slip plate. For the description of the inside of the plate boundary layer, the terms in parentheses are replaced by functions of boundary-layer variables (Section 3).

Use of (12) for the total external disturbances has several implications. Since integrals over x_0 in the range $0 < x_0 < x$ are avoided, it is assumed that disturbances near x will not include residual disturbances created as eigenmodes in the boundary layer near x_0 upstream. Equation (12) provides the forced response, but not the eigenmodes. A description of eigenmode generation along the plate requires a subsequent study.

Insertion of the plate on the point disturbance source wake displaces the ambient flow and modifies the station at which the wake centerline enters the plate boundary layer. This correction for nonparallel flow is needed in the freestream, where $x - x_0$ is of order x, but is not needed inside the boundary layer, where the flow is parallel. Outside the boundary layer, the ambient velocity components are assumed to be (U, 0), when, in fact, they are $(U, U\beta/2R)$, where β is a constant (≈ 1.7208) associated with the

18

Blasius function. Therefore, a source actually located at x_0 and y_0 is moved to the apparent location x_0 and $y_0 + \beta x/R$, from whence the above equations can be applied. Only when the source wake is too distant to have met the boundary layer at x does this simple shift fail.

3. Boundary-layer disturbances for any external source

The disturbance stream function caused by the contact of a wave of given wavenumber with a boundary-layer edge is assumed to have the form

$$\psi = e^{ikx - i\omega t} \phi(\eta) \qquad \eta \equiv \frac{yR}{x} \qquad (13)$$

in the boundary layer. Only one value of streamwise wavenumber k is useful for given l and ω. That value is $k \approx \omega/U$, if $x - x_0 > 0$. Substitution into the Oseen form of the vorticity transport equation indicates that this is one of two possible values. The other pertains when $x - x_0 < 0$ (downstream source with upstream influence, a problem not addressed here). A normalized streamwise wavenumber component K is defined:

$$\frac{kx}{R} \equiv K \sim \Omega + iR^{-1}(\Omega^2 + L^2) \qquad (14)$$

It is well known that a leading approximation for $\phi(\eta)$ that is uniformly valid for values of η up to order one can be obtained for this parameter domain by solving the Orr-Sommerfeld equation.

$$\left(f_\eta - \frac{\Omega}{K}\right)\left(\phi_{\eta\eta} - K^2\phi\right) - f_{\eta\eta\eta}\phi = (iKR)^{-1}\left(\phi_{\eta\eta\eta\eta} - 2K^2\phi_{\eta\eta} + K^4\phi\right) \qquad (15)$$

where f is the Blasius function, defined as mean-stream function over $(\nu Ux)^{1/2}$.

21

In fact, solutions of the Orr-Sommerfeld equation are valid descriptions for any η less than order $\ln \Omega R$. Fortunately, the largest η that must be considered that is not in the freestream is only of order $(\ln \Omega R)^{1/2}$. Boundary conditions are $\phi(0) = \phi_\eta(0) = 0$, and as $\eta \to \infty$, $\phi \sim \exp(iL\eta)$ plus additional waves of bounded variation.

The main advantage of the present asymptotic theory for large R is that not all terms in (15) are needed everywhere. Thus, the following flow layers are described separately: a wall layer, where η is of order $(\Omega R)^{-1/2}$; the main boundary layer where η is of order one; an edge layer, where η is of order $(\ln \Omega R)^{1/2}$; and the freestream. Only the leading approximation in each subregion is of interest. (The perturbation term of order R^{-1} in (14) is needed only in the edge layer, where it provides a *first-order estimate of the* contents of the first parentheses in (15). Elsewhere, $K \approx \Omega$.)

3.1 Wall layer: $\eta = O(\Omega R)^{-1/2}$

As in the asymptotic stability theory, there is a thin layer adjoining the surface in which the highest derivative is needed in order to satisfy homogeneous conditions at the surface. To leading order in R^{-1}, (15) reduces to

$$-\phi_{\eta\eta} = (i\Omega R)^{-1} \phi_{\eta\eta\eta\eta} \tag{16}$$

when η is of order $(\Omega R)^{-1/2}$. The solution that satisfies $\phi(0) = \phi_\eta(0) = 0$ and that does not grow exponentially as η approaches order one is

$$\phi = C \left\{ -1 + (1-i)\, \eta \left(\frac{\Omega R}{2}\right)^{1/2} + \exp\left[(-1+i)\, \eta \left(\frac{\Omega R}{2}\right)^{1/2}\right] \right\} \tag{17}$$

22

The scale factor C will be determined by matching with the boundary-layer function. From this sublayer profile, the transformed surface shear is given by

$$\phi_{yy}(0) = -\frac{iC\Omega R^3}{x^2} \tag{18}$$

The maximum disturbance velocity component in this layer occurs in the streamwise direction when $\eta(\Omega R)^{1/2} = 3.23$. That value is

$$|\phi_{y,max}| = 1.069\,|C|\,(\Omega R)^{1/2}\,\frac{R}{x} \tag{19}$$

The wall layer profile of normalized $|\phi_y|$ is shown in figure 2. This minor maximum is shown in figures 5 and 6 of (Rogler and Reshotko 1975) also.

3.2 The main boundary layer: $\eta = O(1)$

When both η and $f_{\eta\eta}$ are of order one, the right member of (15) can be omitted, and the governing equation is known as the Rayleigh equation (with phase speed equal to ambient speed):

$$(f_\eta - 1)(\phi_{\eta\eta} - \Omega^2\phi) - f_{\eta\eta\eta}\phi = 0 \tag{20}$$

In order to match the sublayer profile, it is required that, when η is of order one and $\eta \to 0$,

$$\phi \to 0 \qquad \phi_\eta \to C(1-i)\left(\frac{\Omega R}{2}\right)^{1/2} \tag{21}$$

23
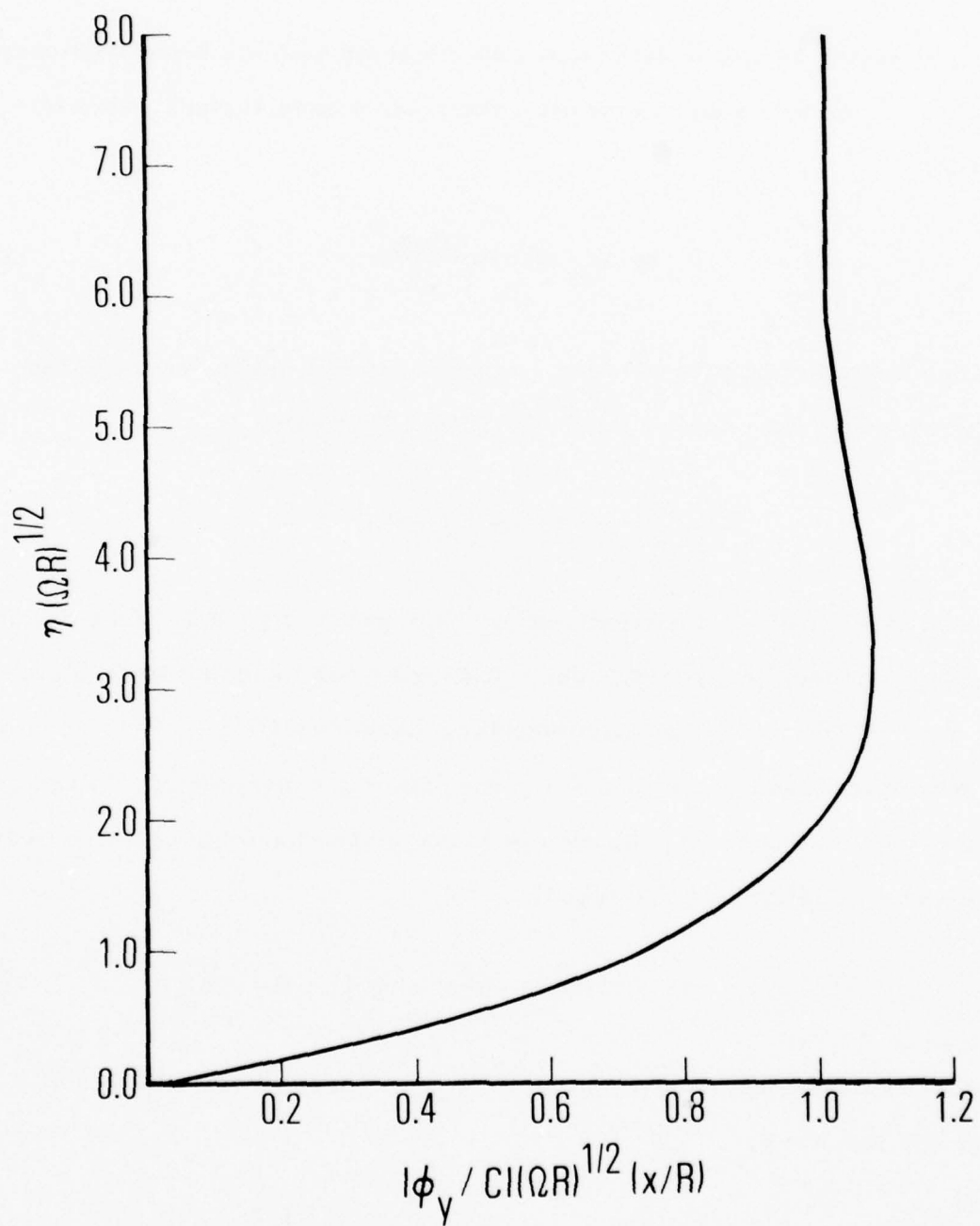
Figure 2. Streamwise Disturbance Profile in Wall Layer

The scale factor C remains to be found by matching the calculated boundary-layer profile with that in an edge layer to be described.

Numerical integration of the Rayleigh equation indicates that the velocity components both increase monotonically in the main boundary layer with the streamwise component always larger than the normal component. Limiting profiles of ϕ_η (proportional to streamwise velocity component) are

$$\frac{\phi_\eta}{\phi_\eta(0)} \sim \begin{cases} (1 - f_\eta)^{-1} - f_{\eta\eta} \displaystyle\int_0^\eta (1 - f_\eta)^{-2} \, d\eta & \Omega \ll 1 \quad (22a) \\ \\ \cosh \Omega\eta & \Omega \gg 1 \quad (22b) \end{cases}$$

These and intermediate Ω profiles are shown in figure 3. A second approximation in the low-frequency limit, for which (22a) is the first approximation will be used in figure 4 and is developed in Appendix A.

At the outer edge of the boundary layer, the Blasius mean velocity and shear profiles have an exponential asymptotic form given by

$$1 - f_\eta \sim \frac{\gamma_1}{H} e^{-H^2} \left[1 - \frac{1}{2H^2} + \frac{1 \cdot 3}{(2H^2)^2} - \frac{1 \cdot 3 \cdot 5}{(2H^2)^3} + \cdots \right] \tag{23}$$

$$f_{\eta\eta\eta} \sim -\gamma_1 H e^{-H^2} + \text{TST} \tag{24}$$
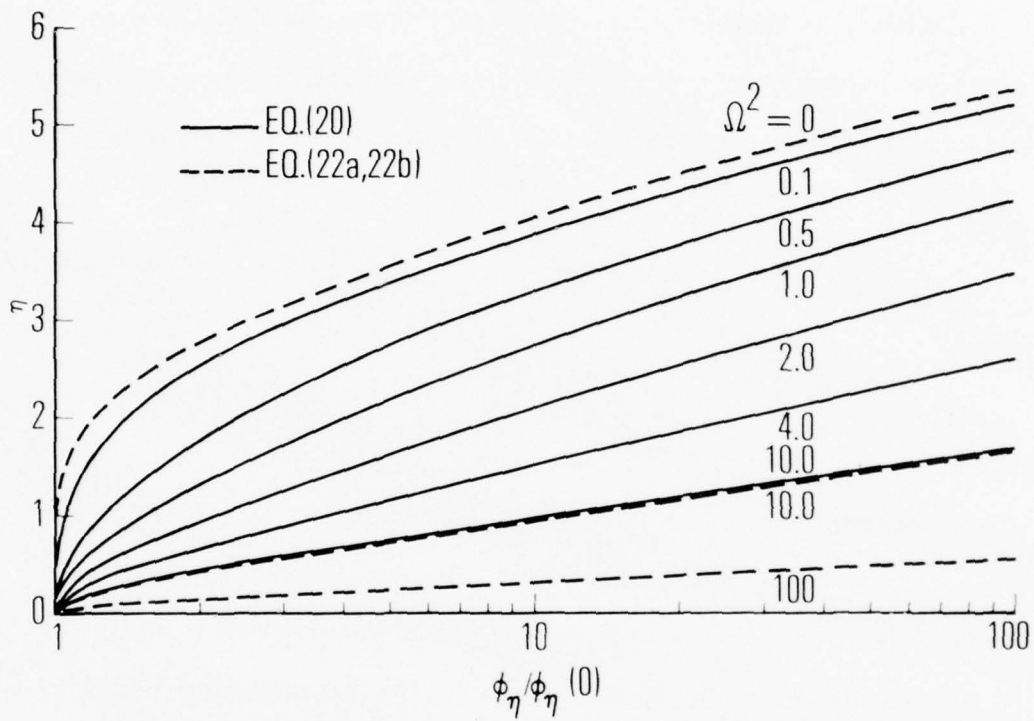
Figure 3. Streamwise Disturbance Profile in Boundary Layer
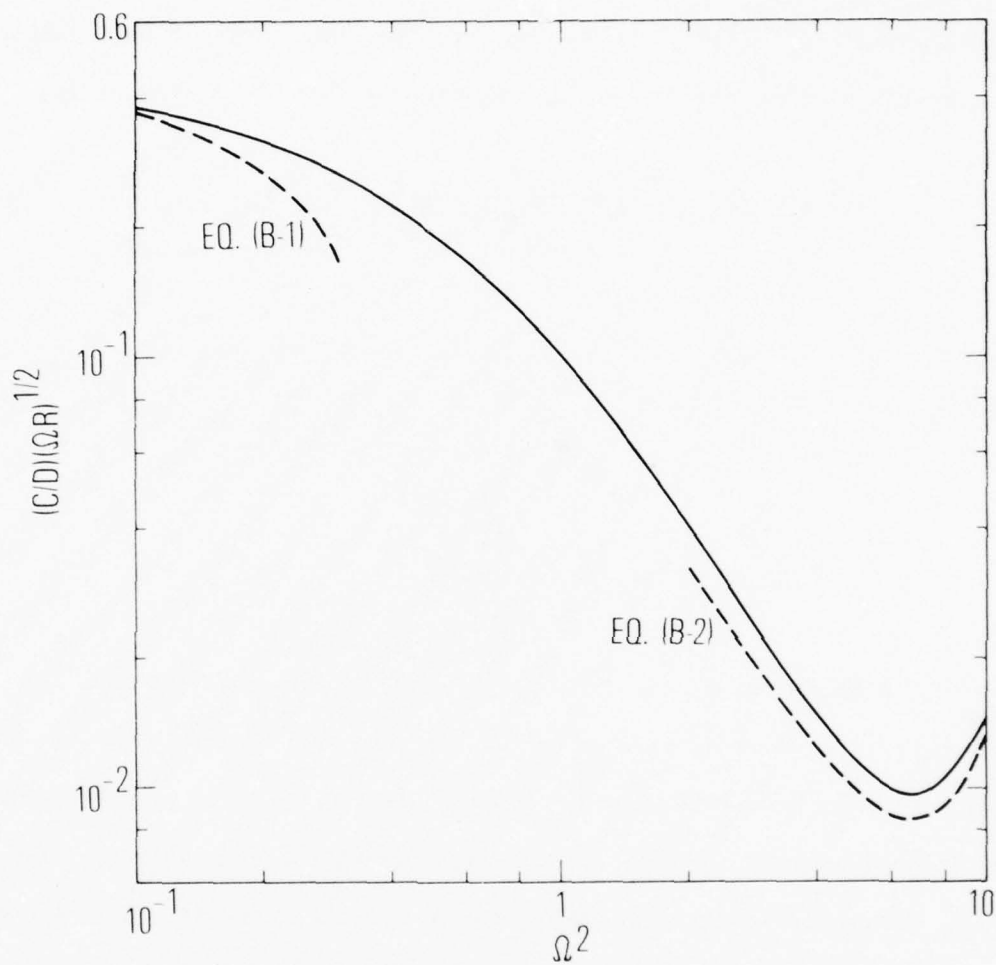
Figure 4. Amplitude Ratio Across Boundary Layer

where $H \equiv (\eta - \beta)/2$ and TST refers to transcendentally small terms. γ_1 is a Blasius constant ≈ 0.23373. When these coefficient functions are used in (20), ϕ approaches a parabolic cylinder function as $\eta \to \infty$. Specifically,

$$\phi \sim D \frac{1 - i}{\sqrt{2}} H^{\Omega^2} e^{H^2} \left[1 + \frac{p_1}{2H^2} + \frac{p_2}{(2H^2)^2} + \frac{p_3}{(2H^2)^3} + \cdots \right] \qquad (25)$$

where

$$4 p_1 = 2 + \Omega^2 (\Omega^2 - 1)$$

$$8 p_2 = (\Omega^4 - 5\Omega^2 + 8) p_1 - 10$$

$$12 p_3 = (\Omega^4 - 9\Omega^2 + 22) p_2 - 10 p_1 + 74$$

and where D is introduced as a scale parameter for the outer edge of the boundary layer. It must be related to C, its inner edge counterpart, so that disturbances in the wall layer can be scaled. D will be found by matching (25) with its corresponding expansion obtained from the edge layer. The ratio C/D, obtained by numerical integration of (20), is plotted in figure 4. Because (20) has real coefficients, C/D is real. Also shown are the low- and high-frequency forms obtained in Appendix A.

3.3 Edge layer: $\eta = O[\ln(\Omega R)]^{1/2}$

Equation (20) is inadequate when η becomes logarithmically large; specifically, when $H \approx H_e$, where

28

$$H_e^3 \, e^{H_e^2} = \gamma_1 \Omega R \gg 1 \qquad (26)$$

There, the terms in the Rayleigh equation have become as small as the largest viscous term in the Orr-Sommerfeld equation. H_e and $\eta_e = 2H_e + \beta$ are plotted in figure 5.

The subregion where H^2 is in the neighborhood of H_e^2 is called an edge layer. It can be considered to be simply a critical layer from asymptotic stability theory in the limit where the phase speed has increased to equal the ambient speed. The dimensionless edge-layer thickness here is much larger than the thickness, $\approx (\Omega R)^{-1/3}$, of an imbedded critical layer because of the exponential tail of the Blasius flow profile. With the present theory, the edge-layer problem is solved for the first time. A previous attempt was made by Graebel (1966), who, by truncating the mean flow profile at $y = \delta$, concluded erroneously that the thickness of the edge critical layer was of order $(\Omega R)^{-1/4}$.

When H^2 is of order $\log(\Omega R)$, the Orr-Sommerfeld equation can be reduced to

$$\frac{1}{16} \, \phi_{HHHH} + \left[i\gamma_1 \Omega R \left(\frac{1}{H} - \frac{1}{2H^3} + \cdots \right) e^{-H^2} + L^2 - \Omega^2 \right] \frac{\phi_{HH}}{4}$$

$$- \left[\gamma_1 \Omega R \left(H + \frac{\Omega_1^2}{H} - \cdots \right) e^{-H^2} + \Omega^2 L^2 \right] \phi = 0 \qquad (27)$$

29
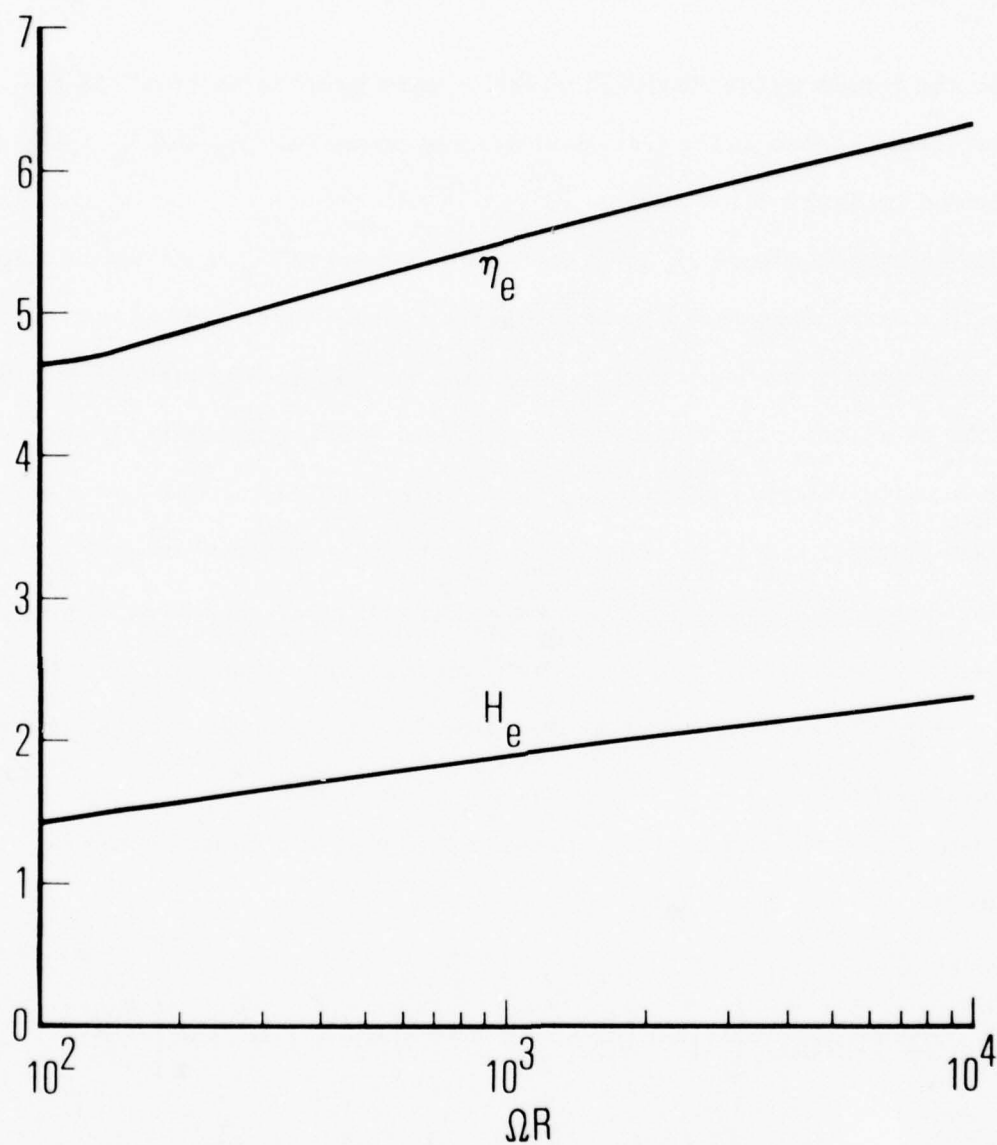
Figure 5. Edge Layer Center Location

30

The least trivial problem results when the edge-layer variable is chosen to be h, where

$$H^2 = H_e^2 + h \tag{28}$$

and h is of order one. Then, in the edge layer, ϕ is represented as an expansion of the form

$$\phi \sim \phi_0(h) + H_e^{-2}\phi_1(h) + H_e^{-4}\phi_2(h) + \cdots \tag{29}$$

where ϕ_0 and ϕ_1 must satisfy

$$\phi_{0,hhhh} + ie^{-h}(\phi_{0,hh} - \phi_0) = 0 \tag{30}$$

$$\phi_{1,hhhh} + ie^{-h}(\phi_{1,hh} - \phi_1) = -2h\phi_{0,hhhh} - 3\phi_{0,hhh} - (L^2 - \Omega^2)\,\phi_{0,hh}$$
$$- (i/2)e^{-h}\left[(h-1)\,\phi_{0,hh} + \phi_{0,h} - (2\Omega^2 + h)\phi_0\right] \tag{31}$$

Equation (29) is in inverse powers of H_e^2, but the true error is even larger, of order H_e^{-1} since the Orr-Sommerfeld equation has already omitted a nonparallel flow term containing the third derivative. The missing term is the $V\psi_{yyy}$ term from the vorticity transport equation. This omission means that the parallel-flow assumption in this application carries an error of order $[\log(\Omega R)]^{-1/2}$. A numerical estimate of the size of this error can

31

be obtained by substitution. Thus, when Ω is one and the x-Reynolds number is the minimum critical value from stability theory (60,000), $[\log(\Omega R)]^{-1/2}$ is 0.43. Disturbance profile shapes in other layers do not carry such a large error, but disturbance amplitude levels do.

The Blasius function $f_{\eta\eta\eta}$ for mean velocity curvature is not a valid estimate if η is too large. The mean curvature is needed as a coefficient in the Orr-Sommerfeld equation. Goldstein (1956, 1960) and Imai (1957) have shown the error in Blasius functions to be of order $R^{-2} \log R^2$ when η is of order one. It seems reasonable that the relative error in $f_{\eta\eta\eta}$, where $f_{\eta\eta\eta}$ decays as $\exp(-H^2)$, may reach order one when H^2 is approximately $\log(R^2)$. In the edge layer, however, H^2 is only order $\log(\Omega R)$; therefore, the relative error in $f_{\eta\eta\eta}$ there should be no more than order roughly $1/R$.

Four solutions for the fourth-order equation (30) with variable coefficients are developed in Appendix B. These are $\phi_0^{(1)}$, $\phi_0^{(2)}$, $\phi_0^{(3)}$, and $^{(2)}\phi_0$. The first three are found by recognizing expansions about $h = \infty$. The fourth is derived from an expansion about $h = -\infty$. As $h \to -\infty$ (boundary-layer side), the four edge-layer solutions become

$$\phi_0^{(1)} \sim i e^{-h} \tag{32}$$

$$\phi_0^{(2)} \sim i e^{-h} J_0 \left[2 (i e^{-h})^{1/2} \right] \tag{33}$$

$$\phi_0^{(3)} \sim (-\pi i + 2 + 4\gamma) \phi_0^{(2)} + (-6.46404 + i\, 6.76836) \phi_0^{(1)} \tag{34}$$

$$^{(2)}\varphi_0 \sim e^h \tag{35}$$

where γ is Euler's constant (≈ 0.577). In this limit, $\varphi_0^{(2)}$ and $\varphi_0^{(3)}$ grow too rapidly to be separately useful in the boundary layer. These two solutions asymptotically satisfy the differential equation

$$\varphi_{0,hhhh} + ie^{-h}\,\varphi_{0,hh} \sim 0 \tag{36}$$

instead of the second-order equation

$$\varphi_{0,hh} - \varphi_0 \sim 0 \tag{37}$$

which is compatible with the boundary-layer expansions. For this reason, and for compatibility with the boundary-layer scaling parameter D, the four solutions are combined (weighted) as follows:

$$\varphi_0 \sim E\left[\varphi_0^{(3)} + (\pi i - 2 - 4\gamma)\,\varphi_0^{(2)} + (6.46404 - i\,6.76836)\,\varphi_0^{(1)}\right]$$

$$+ D\,\frac{1-i}{\sqrt{2}}\,\gamma_1\,\Omega RH_e^{\Omega^2-3}\,{}^{(2)}\varphi_0 \tag{38}$$

Coefficients D and E remain to be found by matching with freestream expansions.

As $h \to +\infty$ (freestream side), the four edge-layer solutions become

33

$$\phi_0^{(1)} \sim 1 + TST \qquad (39)$$

$$\phi_0^{(2)} \sim h + TST \qquad (40)$$

$$\phi_0^{(3)} \sim h^2 + TST \qquad (41)$$

$$^{(2)}\phi_0 \sim (i/3)\,h^3 + e_2 h^2 + e_1 h + e_0 + TST \qquad (42)$$

where e_0, e_1, and e_2 are constants that are given in Appendix B. Then, the leading-order solution can be written

$$\phi_0 \sim f_3 h^3 + f_2 h^2 + f_1 h + f_0 + TST \qquad (43)$$

where

$$f_3 = D\,\frac{1+i}{3\sqrt{2}}\left(\gamma_1^{\Omega} RH_e^{\Omega^2} - 3\right) \qquad (44)$$

$$f_2 = E + D\,\frac{1-i}{\sqrt{2}}\,\gamma_1^{\Omega} RH_e^{\Omega^2} - 3\,e_2 \qquad (45)$$

$$f_1 = E\,(\pi i - 2 - 4\gamma) + D\,\frac{1-i}{\sqrt{2}}\,\gamma_1^{\Omega} RH_e^{\Omega^2} - 3\,e_1 \qquad (46)$$

$$f_0 = E\,(6.46404 - i\,6.76836) + D\,\frac{1-i}{\sqrt{2}}\,\gamma_1^{\Omega} RH_e^{\Omega^2} - 3\,e_0 \qquad (47)$$

34

Solutions of higher order were not sought: nevertheless, from (31) and a corresponding equation for ϕ_2 the asymptotic behavior as $h \to \infty$ can be established to be

$$\phi_1 \sim -6f_3 (L^2 - \Omega^2) \frac{h^5}{5!} - \left[18f_3 + 2f_2 (L^2 - \Omega^2) \right] \frac{h^4}{4!} + \text{cubic} \tag{48}$$

$$\phi_2 \sim (L^4 - \Omega^2 L^2 + \Omega^4) \left(6f_3 \frac{h^7}{7!} + 2f_2 \frac{h^6}{6!} \right) + 42f_3 (L^2 - \Omega^2) \frac{h^6}{6!} + \text{quintic} \tag{49}$$

3.4 Freestream: $\eta - \eta_e = O(1)$

Equation (27) contains the few terms needed in the ambient flow where the differential equation has constant coefficients:

$$\phi_{\eta\eta\eta\eta} + (L^2 - \Omega^2) \phi_{\eta\eta} - \Omega^2 L^2 \phi = 0 \tag{50}$$

The solution desired is

$$\phi \sim e^{iL\eta_e} \left[e^{iL(\eta - \eta_e)} + C_r e^{-iL(\eta - \eta_e)} + C_w e^{-\Omega(\eta - \eta_e)} \right] \tag{51}$$

The parameters C_r and C_w are more convenient than C_r^* and C_w^* used in (12). The coefficient of the first modal function $[\exp (iL\eta)]$ has been normalized as indicated after (15). A fourth modal function $[\sim \exp(\Omega\eta)]$ has been omitted in order to satisfy the other of two boundary conditions at ∞; namely, that $|\phi|$ not grow with η in the freestream. The second and third

35

modes retained can be interpreted as a reflected wave of relative amplitude C_r to be determined and a potential-flow response, which is a streamwise wave entirely. Lack of decay as $\eta \to \infty$ in the amplitude of the reflected wave is acceptable because the exponent depends on wavenumber, which is the integration variable for the inverse Fourier transform.

In order that the edge-layer expansion given by (29), (43), (48), and (49), match (51), the edge-layer expansion is written in the freestream variable $\eta - \eta_e$ by means of

$$h = H_e \, (\eta - \eta_e) + \left(\frac{1}{4}\right) (\eta - \eta_e)^2 \tag{52}$$

Upon substitution, the edge-layer expansion becomes

$$
\begin{aligned}
\phi \sim\ & f_3 \left[H_e^3 (\eta - \eta_e)^3 + \frac{3}{4} H_e^2 (\eta - \eta_e)^4 + \cdots \right] + f_2 H_e^2 (\eta - \eta_e)^2 + \cdots \\
& + \frac{1}{H_e^2} \left\{ -6f_3 (L^2 - \Omega^2) \frac{1}{5!} \left[H_e^5 (\eta - \eta_e)^5 + \frac{5}{4} H_e^4 (\eta - \eta_e)^6 + \cdots \right] \right. \\
& \left. - \left[18f_3 + 2f_2 (L^2 - \Omega^2) \right] \frac{1}{4!} \left[H_e^4 (\eta - \eta_e)^4 + \cdots \right] \right\} \\
& + \frac{1}{H_e^4} \left\{ 6f_3 (L^4 - \Omega^2 L^2 + \Omega^4) \frac{1}{7!} \left[H_e^7 (\eta - \eta_e)^7 + \frac{7}{4} H_e^6 (\eta - \eta_e)^8 + \cdots \right] \right. \\
& + 2f_2 (L^4 - \Omega^2 L^2 + \Omega^4) \frac{1}{6!} H_e^6 (\eta - \eta_e)^6 + \cdots \\
& \left. + 42f_3 (L^2 - \Omega^2) \frac{1}{6!} H_e^6 (\eta - \eta_e)^6 + \cdots \right\} + \cdots
\end{aligned}
\tag{53}
$$

Only two orders H_e^3 and H_e^2 have been retained because only the leading-order solution in Appendix B was developed, and higher-order solutions appear at the next order. Equation (53) must match the expansion of (51) for small $\eta - \eta_e$, which is

$$\varphi \sim e^{iL\eta_e} \sum_0^\infty \frac{(\eta - \eta_e)^k}{k!} \left[(iL)^k + (-iL)^k C_r + (-\Omega)^k C_w \right] \qquad (54)$$

Since (53) does not contain terms containing $(\eta - \eta_e)^0$ or $(\eta - \eta_e)^1$, such terms in (54) must vanish by a proper choice of C_r and C_w, thus

$$C_r = -\frac{\Omega + iL}{\Omega - iL}, \qquad C_w = \frac{2iL}{\Omega - iL} \qquad (55)$$

In addition,

$$f_2 = iH_e^{-2} L (\Omega + iL) e^{iL\eta_e} \qquad (56)$$

and

$$f_3 = -\left(\frac{i}{3}\right) H_e^{-3} \Omega L (\Omega + iL) e^{iL\eta_e} \qquad (57)$$

were chosen to match powers of $(\eta - \eta_e)^2$ and $(\eta - \eta_e)^3$. Higher powers (four through seven) also match to leading order. The asymptotic variation of the higher-order functions φ_1 and φ_2 was unnecessarily

37

displayed in (53) as a confirmation of the adequacy of the matching procedure. Substitution of (56) and (57) into (44) and (45) indicates that

$$E \sim f_2 \sim i H_e^{-2} L \, (\Omega + iL) \, e^{iL\eta}e \qquad (58)$$

$$D \sim - \frac{1 + i}{\sqrt{2}} \, \frac{\Omega L (\Omega + iL)}{\gamma_1^{\Omega} R H_e^2} \, e^{iL\eta}e \qquad (59)$$

and that none of the constants e_2, e_1, or e_0 is needed.

When coefficients E and D are replaced in (38), in the edge layer proper, where $\phi_0^{(i)}$ are all of comparable magnitude, the term with E is theoretically larger than that with D, by a factor of the "large" parameter H_e. Thus, E scales the edge-layer disturbances, and (C/D)D scales disturbances in the boundary layer and sublayer. The leading-order edge-layer solution, from (38) and Appendix B is, therefore, the closed-form expression

$$\frac{\phi_0}{E} = (6.46404 - i\,6.76836)(1 + ie^{-h}) + f(2e^{-h/2}) \qquad (60)$$

where f(x) is given by (B-37). The magnitude and phase of ϕ_0/E, which is proportional to the transverse velocity component, and $\phi_{0,h}/E$, which is proportional to the streamwise disturbance velocity component, are plotted in figures 6a and 6b, respectively. The maximum disturbance velocities occur in the freestream, not in the edge layer. Further, the vertical component of disturbance velocity, which was numerically negligible compared
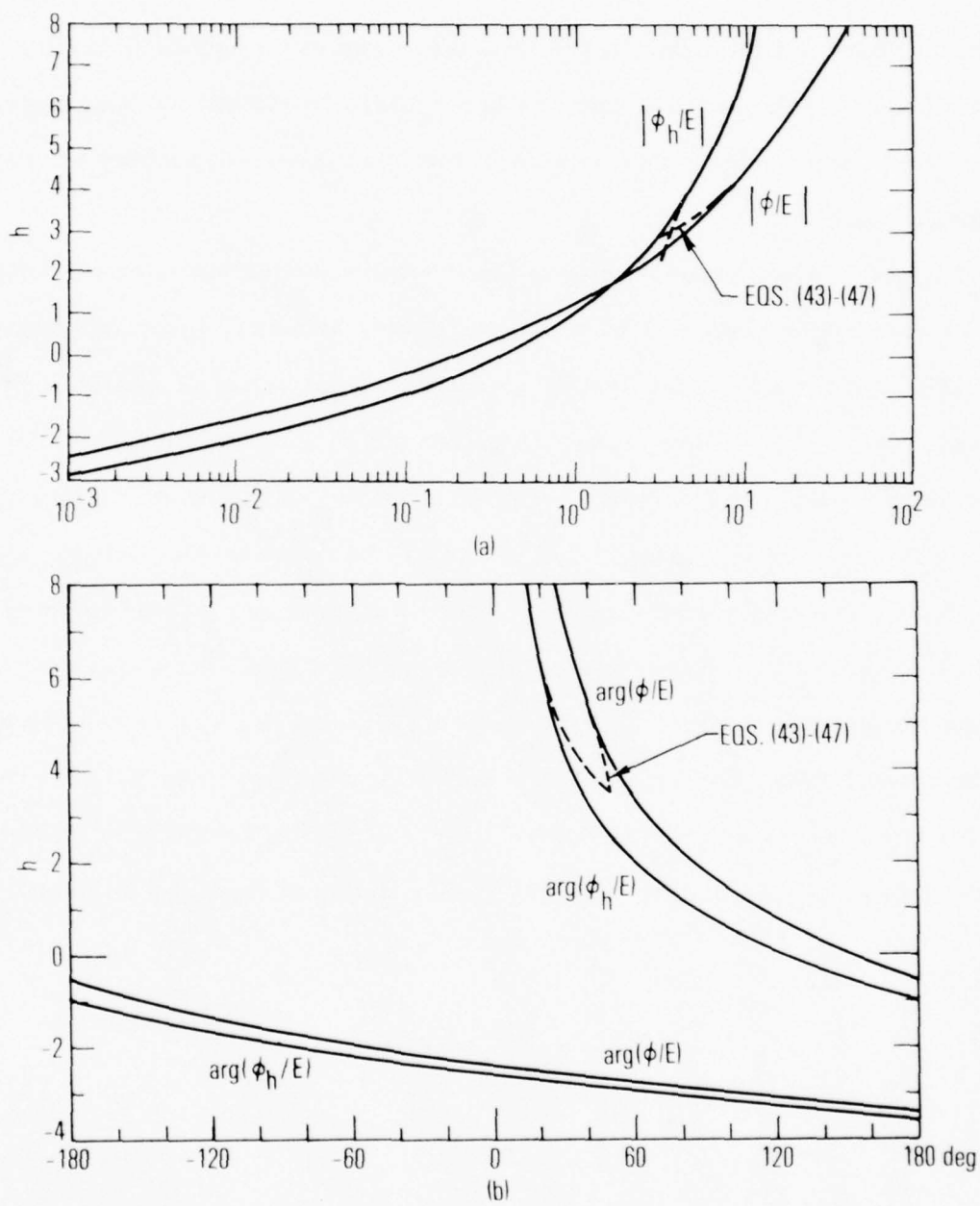
Figure 6. Edge Layer Profiles: (a) Magnitude (b) Phase

to the horizontal component in the wall layer and main boundary layer, finally becomes comparable with the horizontal component and may exceed the latter in size in the outer portion of the edge layer, depending on their relative scales.

Figure 7 is a composite plot of the streamwise perturbation velocity profile in the three layers into which the steady boundary layer is divided by this asymptotic theory. φ_η (which depends on y but not ℓ) is multiplied by a transform $\Psi^{(y)}$ (which depends upon ℓ but not y) and then integrated over ℓ to obtain a dimensional velocity. The integral of $\Psi^{(y)}$ $d\ell$ serves merely as a scale factor, one that depends on the nature of the external disturbance. The specific relationship between the three sublayer profiles depends only on Ω, R, x_0, and y_0. Experimentally obtained profiles with a vibrating ribbon (Kachanov, Kozlov, and Levchenko 1976) and numerical results with a convected lattice (Rogler and Reshotko 1975) (figures 5 and 6) both exhibit the features of this composite profile, i.e., a slight overshoot in a thin sublayer and very rapid growth with increasing distance from the surface.

Figure 7.   Streamwise Disturbance Profile
in Boundary Layer (Montage)

4. Results

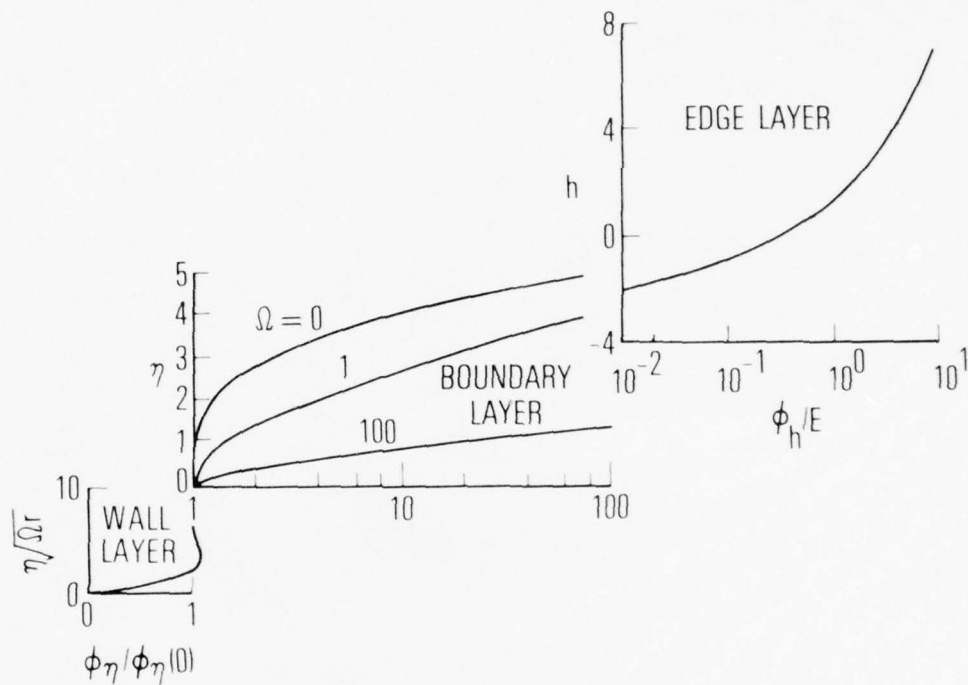Disturbances in the presence of a semi-infinite flat plate, generated as described in Section 2 by an external oscillating source of vorticity (and limited to the forced response as opposed to eigenmodes), are plotted for two locations: the freestream and the wall-layer edge.

In these applications, it is necessary to adjust the disturbance scale differently, depending on which disturbance velocity component is desired. Specifically, the transverse disturbance velocity in the presence of the plate is

$$\exp\left[i\omega\left(t - \frac{x - x_0}{U}\right)\right]\frac{\partial \psi}{\partial x} = \frac{1}{2\pi}\int_{-\infty}^{\infty} \phi(\eta)\ \Psi^{(x)}\left(\frac{R}{x}\right) dL \tag{61}$$

since the limit $\phi(\eta) \rightarrow \exp(iL\eta)$ plus bounded terms is required in the freestream and since $\partial\psi/\partial x$ is proportional to $\phi(\eta)$ rather than its derivative.

The streamwise component, $\partial\psi/\partial y$, proportional to ϕ_η is obtained from (51) of Section 3. In the freestream, the form

$$\phi_\eta = iL\left[e^{iL\eta} - C_r e^{2iL\eta} e^{-iL\eta} - \frac{\Omega C_w}{iL} e^{(\Omega + iL)\eta} e^{-\Omega\eta}\right] \tag{62}$$

is compatible with (11) if the streamwise component is

$$\exp\left[i\omega\left(t - \frac{x - x_0}{U}\right)\right]\frac{\partial \psi}{\partial y} = \frac{1}{2\pi}\int_{-\infty}^{\infty} \frac{\phi_\eta}{iL}\ \Psi^{(y)}\left(\frac{R}{x}\right) dL \tag{63}$$

Equations (61) and (63) correspond to (11), which applied in the absence of the plate.

4.1 Freestream profiles

Profiles of disturbance velocity components in the freestream are desired both for comparison with recent experimental profiles obtained behind a vibrating ribbon (Kachanov, Kozlov, and Levchenko 1976) and because disturbances there are the largest. The combination of (51), (55), and (61) through (63) resulted in the closed-form profiles:

$$
\frac{U}{\dot{\Gamma}} \left| \begin{Bmatrix} \partial\psi/\partial y \\ \partial\psi/\partial x \end{Bmatrix} \right| = \frac{1}{\pi} e^{-\Omega_0^2} \left| \begin{Bmatrix} S_1 (Y - Y_0) + S_1 (Y + Y_0 - 2Y_e) \\ C_1 (Y - Y_0) + C_1 (Y + Y_0 - 2Y_e) \end{Bmatrix} \right.
$$
$$
+ 2 \left[C_1 (Y + Y_0 - 2Y_e) - C_2 (Y + Y_0 - 2Y_e) - S_2 (Y + Y_0 - 2Y_e) \right]
$$
$$
+ 2e^{-(Y - Y_e)} \left. \left[-C_1 (Y_0 - Y_e) + C_2 (Y_0 - Y_e) + S_2 (Y_0 - Y_e) \right] \right|
$$

$$(64)$$

where

$$
\Omega_0^2 \equiv \omega^2 \nu \left(\frac{x - x_0}{U^3} \right) \qquad Y \equiv y \frac{\omega}{U}
$$

$$(65)$$

and where C_1, S_1, C_2, S_2 are integrals defined by

$$
\begin{Bmatrix} C_k (x) \\ S_k (x) \end{Bmatrix} = \int_0^\infty \frac{e^{-\Omega_0^2 t^2}}{(t^2 + 1)^k} \begin{Bmatrix} \cos (xt) \\ t \sin (xt) \end{Bmatrix} dt
$$

$$(66)$$

44

and evaluated by parameter differentiation. The closed-form results are

$$\begin{Bmatrix} C_1(x) \\ S_1(x) \end{Bmatrix} = \frac{\pi}{4} e^{\Omega_0^2} \left[e^{-x} \operatorname{erfc}\left(\Omega_0 - \frac{x}{2\Omega_0}\right) \begin{Bmatrix} + \\ - \end{Bmatrix} e^{x} \operatorname{erfc}\left(\Omega_0 + \frac{x}{2\Omega_0}\right)\right] \qquad (67)$$

$$C_2(x) = \left(-\Omega_0^2 + \frac{1}{2}\right) C_1(x) + \left(\frac{x}{2}\right) S_1(x) + \pi^{1/2}\left(\frac{\Omega_0}{2}\right) \exp\left(-\frac{x^2}{4\Omega_0^2}\right) \qquad (68)$$

$$S_2(x) = -\Omega_0^2 S_1(x) + \left(\frac{x}{2}\right) C_1(x) \qquad (69)$$

Streamwise perturbation profiles are compared in figure 8 with experimental measurements obtained (Kachanov, Kozlov, and Levchenko 1976) behind a vibrating ribbon in the presence of a plate. As described in a lecture at Virginia Polytechnic Institute, the experiment was performed at a frequency of 114 Hz and an ambient speed of 532 cm/sec. The ribbon location was not specified. (Its location is not critical, and it has been assumed to lie above the leading edge.) The mean boundary-layer "edge" and surface were located at δ, and S, respectively. The theoretical $y_e - y_0$ (the minimum coordinate plotted) was optimized. The arbitrary amplitude scaling is the same at all stations.

Figure 8 indicates that the characteristic diffusion width is only half of the theoretical value and that the decay is much more rapid. Since these discrepancies would also occur in the absence of a plate, either (5) is wrong, which seems most unlikely, or the experimental frequency must have been
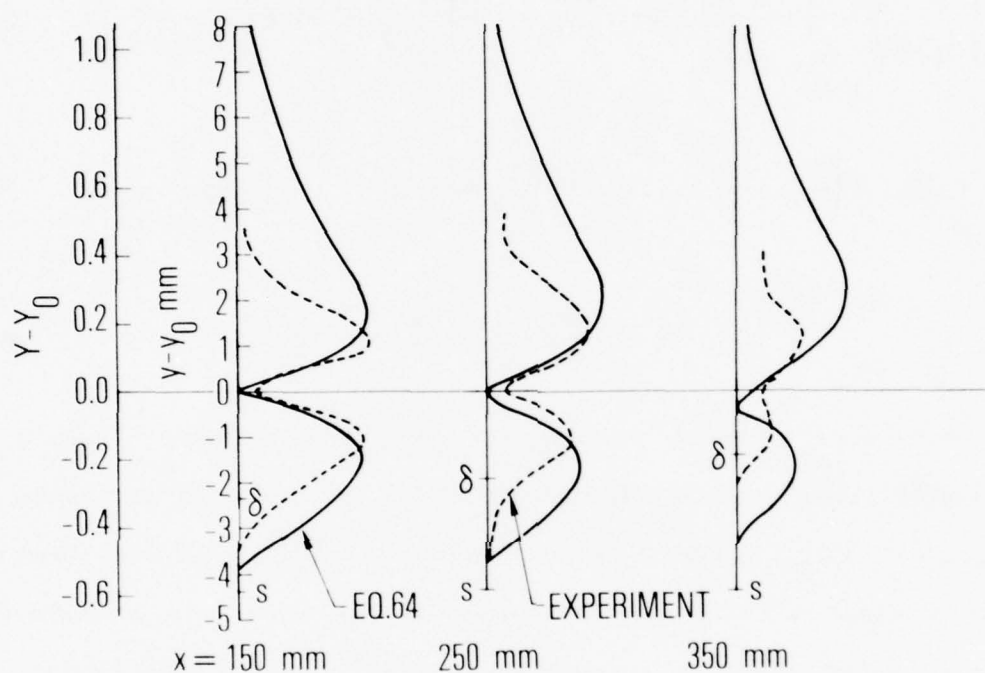
45

Figure 8. Streamwise Disturbance Profiles Outside Boundary
Layer (w = 716 rad/sec, v = 532 cm/sec)

twice the reported 114 Hz. If it is the latter, quantitative as well as qualitative agreement could be reported.

4.2 Wall-layer-edge disturbance amplitude

Infinitesimal external disturbances can only cause boundary-layer transition to the extent that they excite boundary-layer instabilities. Since Tollmien-Schlichting waves, i.e., two-dimensional eigenmodes, travel at a phase speed of about one-third the ambient speed, corresponding to a critical layer (of asymptotic stability theory) located near $\eta = 1$, as much or more interest must be focused on the forced-response disturbances of relatively small amplitudes near $\eta = 1$, as in the very much larger amplitudes in the freestream. In this central portion of the main boundary layer, the streamwise component is always much larger in magnitude than the transverse component and is found (figure 3) for any η once the value at the wall-layer edge is known. A plot of the wall-layer edge disturbance is useful therefore.

From (21), (59), and (63),

$$\left| \frac{\partial \psi}{\partial y} \right|_{\eta = 0} = \frac{(C/D)(\Omega R)^{1/2}}{2\pi \gamma_1 \times H_e^{\Omega^2}} \left| \int_{-\infty}^{\infty} (\Omega + iL) \, e^{iL\eta}e \, \Psi^{(y)} \, dL \right| \tag{70}$$

47

Equation (10) then gives

$$\frac{U}{\dot{\Gamma}}\left|\frac{\partial \psi}{\partial y}\right|_{\eta=0} = \frac{(C/D)(\Omega R)^{1/2}\Omega}{2\gamma_1 \, RH_e^{\Omega^2}} \, e^{-(Y_0 - Y_e)}\left|\mathrm{erfc}\left(\Omega_0 - \frac{Y_0 - Y_e}{2\Omega_0}\right)\right.$$

$$\left. - \frac{1}{\sqrt{\pi}\,\Omega_0} \, \exp\left[-\left(\Omega_0 - \frac{Y_0 - Y_e}{2\Omega_0}\right)^2\right]\right| \quad (71)$$

Because the two parameters of the right member Ω_0 and $Y_0 - Y_e$ mingle frequency and position, they are replaced for graphic purposes with parameters that do not. These are Ux_0/ν, Uy_0/ν, and $\omega\nu/U^2$ (which is equal to Ω/R). Then,

$$\Omega_0 = \left(\frac{\omega\nu}{U^2}\right)\left(R^2 - \frac{Ux_0}{\nu}\right)^{1/2} \qquad Y_0 - Y_e = \left(\frac{\omega\nu}{U^2}\right)\left(\frac{Uy_0}{\nu} - R\eta_e\right) \quad (72)$$

Also, $(C/D)(\Omega R)^{1/2}$ is a function of the $R^2 \, (\omega\nu/U^2)^2$ given in figure 4, and H_e and η_e are functions of $R^2\omega\nu/U^2$ given in figure 5.

In figure 9, the disturbance source has been located as far upstream from the leading edge as an observer is downstream from the leading edge, if his local x-Reynolds number is 10^5. The location and the frequency selected are simply representative. The curves in figure 9 then are those that an anemometer should be able to measure if it were located at the wall-layer edge and translated along the plate. The figure indicates that, if the source is located in line with the plate ($Uy_0/\nu = 0$), the amplitude decays
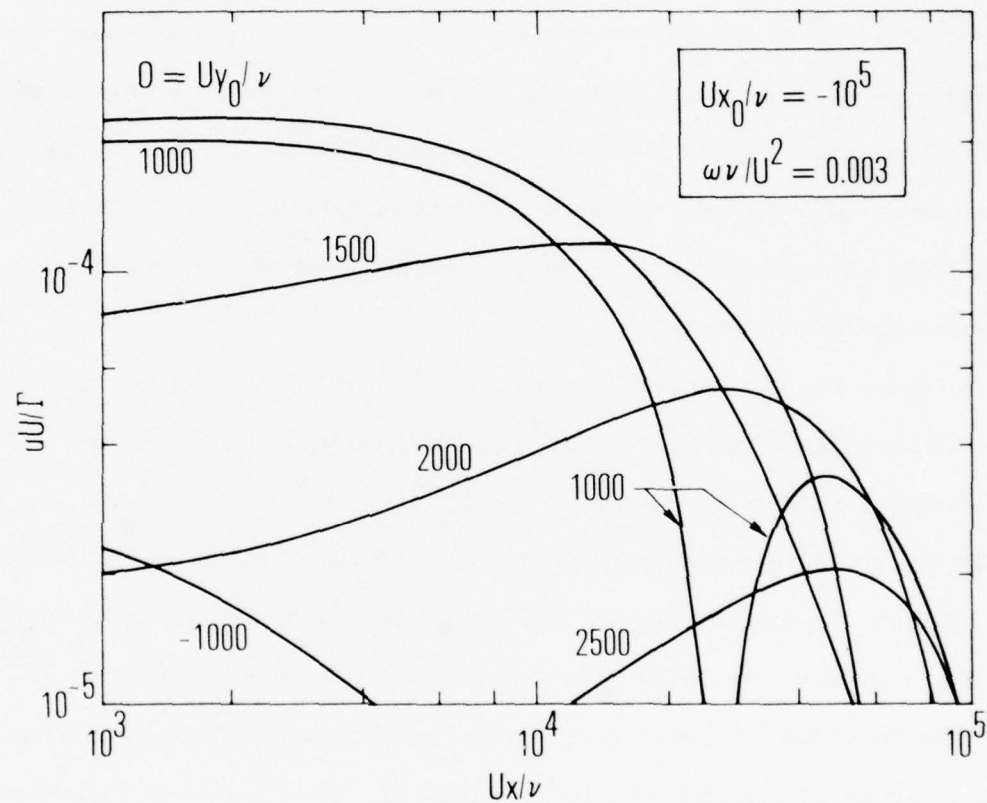
Figure 9. Streamwise Variation of Disturbance Velocity u at Wall-Layer Edge for Various Heights y_0 of Fluctuation Source

49

monotonically downstream. If the source is located below the plate, e.g., $Uy_0/\nu = -1000$, the amplitude in the boundary layer above the plate is greatly reduced. If, however, the source is located on the proximal side so that its wake enters the boundary layer near the stations observed, the amplitude peaks at a finite Reynolds number. (Generally two peaks should be expected, corresponding to the two lobes of the disturbance in the absence of the plate.) The further the plate is from the source wake centerline, the smaller the characteristic disturbance and the greater the Reynolds number of maximum disturbance.

In figure 10, the source has been fixed, and the frequency parameterized. For a station where $Ux/\nu \approx 3 \times 10^4$, the maximum disturbance for $\omega\nu/U^2 = 10^{-3}$ exceeds that for both $\omega\nu/U^2 = 3 \times 10^{-4}$ and 3×10^{-3}.

In figure 11, the observer and the source are both located a distance $10^5 \nu/U$ from the leading edge. The effect of varying frequency is shown. For Uy_0/ν greater than 1000, there is clearly a favored frequency (if perturbation of the boundary layer at that station is desired) or a frequency range to avoid (if a quiescent flow is desired). This behavior indicates the possibility of "detuning" a wind tunnel, perhaps by redesigning the turning-vane chord length to avoid these particularly effective frequencies.
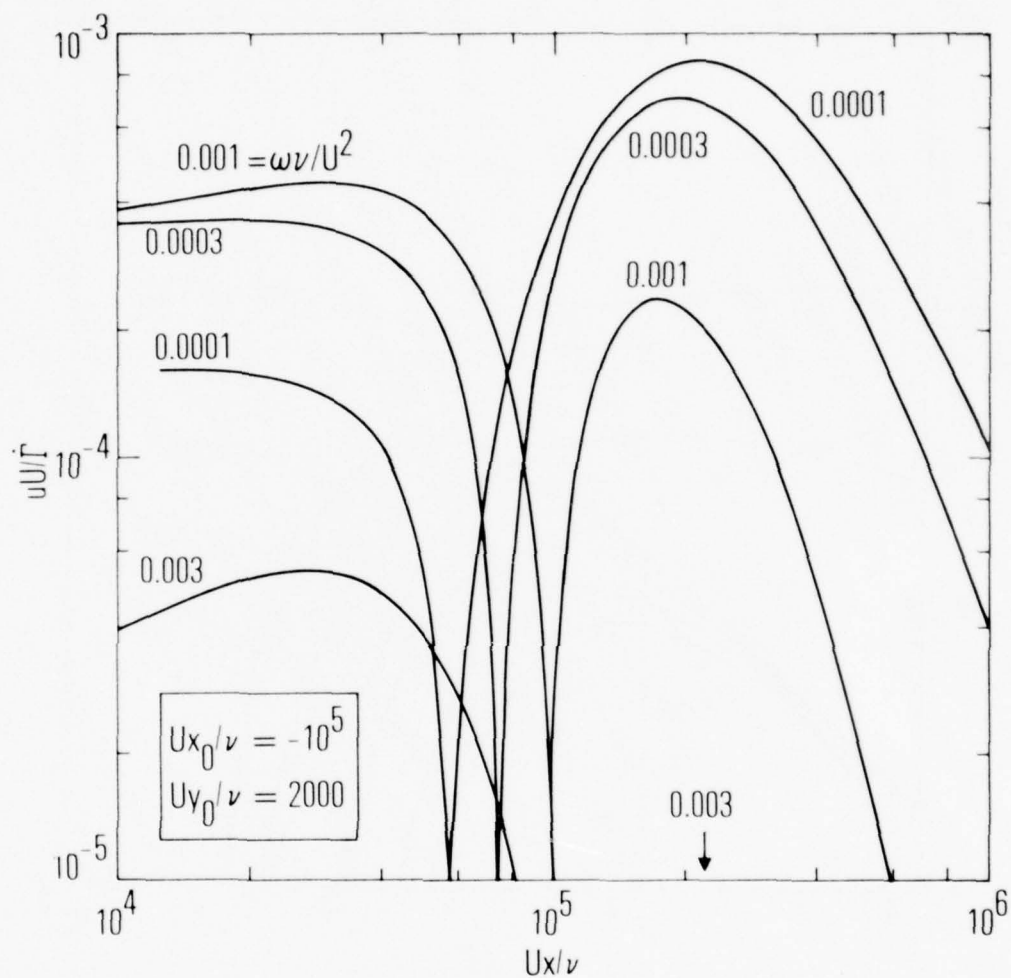
Figure 10.   Streamwise Variation of Disturbance
Velocity u at Wall-Layer Edge
(Various Frequencies)

51
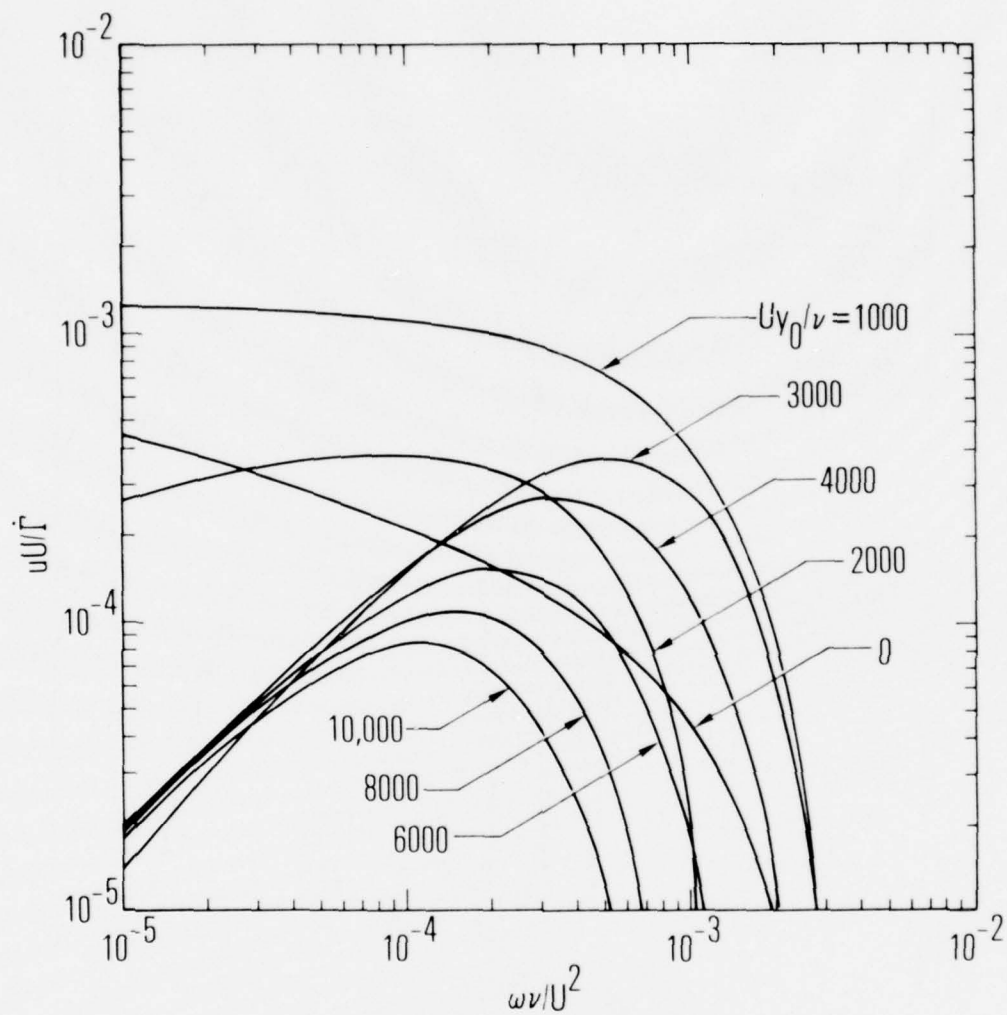
Figure 11. Frequency Variation of Disturbance
Velocity u at Wall-Layer Edge

Appendix A: Limiting forms for $(C/D)(\Omega R)^{1/2}$

The differential equation for disturbance stream function (20), can be solved in both the low- and high-frequency limits. The low-frequency result, which can be verified by substitution, is

$$\frac{\phi}{[\phi_\eta(0)(1 - f_\eta)]} = G(\eta) + \Omega^2 \int_0^\eta [1 - f_\eta(\eta_o)]^2 G(\eta_o) [G(\eta) - G(\eta_o)] d\eta_o + \cdots$$

where

$$G(\eta) \equiv \int_0^\eta [1 - f_\eta(\eta_o)]^{-2} d\eta_o$$

For evaluation of the ratio $(C/D)(\Omega R)^{1/2}$, the behavior of ϕ as $\eta \to \infty$ is needed:

$$\frac{\phi}{[\phi_\eta(0)(1 - f_\eta)]} \sim G(\eta) \left\{ 1 + \Omega^2 \int_0^\eta [1 - f_\eta(\eta_o)]^2 G(\eta_o) d\eta_o \right\} [1 + O(H^{-2})]$$

where $H = (\eta - \beta)/2$. The indicated integration is singular because $G(\eta)$ behaves as

$$G(\eta) \sim (\eta - \beta)^{-1} (1 - f_\eta)^{-2} + \cdots$$

Accordingly, for large η,

$$\int_0^\eta [1 - f_\eta(\eta_o)]^2 G(\eta_o) d\eta_o \sim \log H + c + O(H^{-2})$$

53

where c equals the finite part plus log 2. Specifically,

$$c = \int_0^2 [1 - f_\eta(\eta_o)]^2 \, G(\eta_o) \, d\eta_o + \int_2^\infty \left\{ [1 - f_\eta(\eta_o)]^2 \, G(\eta_o) - (\eta_o - \beta)^{-1} \right\} d\eta_o$$

$$+ \log\left(\frac{2}{2 - \beta}\right)$$

Numerically, $c = 2.125$. Therefore, at low frequencies near the outer edge of the boundary layer,

$$\frac{\phi}{\phi_\eta(0)} \sim (2\gamma_1)^{-1} \, e^{H^2} \left[1 + \Omega^2 \, (\log H + c) + \cdots \right]$$

$$\sim (2\gamma_1)^{-1} \, H^{\Omega^2} e^{H^2} \left[1 + c\Omega^2 + \dots \right]$$

The use of (21) and (25) then gives the boundary-layer amplitude ratio as

$$\left(\frac{C}{D}\right) (\Omega R)^{1/2} \sim (2\gamma_1)(1 - c\Omega^2 + \dots) \qquad \Omega^2 \ll 1. \quad \text{(A-1)}$$

For high frequencies, the $\cosh(\Omega\eta)$ solution, (22b), is not uniformly valid because the third term of (20) becomes important when $H = (\eta - \beta)/2$ is of order Ω. Since the edge layer (Section 3.3) adds viscous complications when H is of order $[\ln(\eta R)]^{1/2}$, the parabolic-cylinder behavior, (25), is only relevant if $\Omega^2 < \ln(\Omega R)$. Equation (25) is essential for the determination of $(C/D)(\Omega R)^{1/2}$, thus, this ratio will be obtained for moderately high frequencies $1 \ll \Omega^2 \ll [\ln(\Omega R)]$.

54

In the notation of Abramowitz and Stegun (1966) when H is of order Ω, φ is a combination $C_1 y_1(\eta - \beta) + C_2 y_2(\eta - \beta)$ of parabolic cylinder functions y_1 and y_2 with parameter $a = \Omega^2 + 1/2$. The $\cosh(\Omega\eta)$ solution for η of order one will match this if C_1 is $\varphi_\eta(0)\exp(\Omega\beta)/(2\Omega)$ and C_2 is $\varphi_\eta(0)\exp(\Omega\beta)/2$. It remains to express y_1 and y_2 in terms of standard solutions U and V, so that the asymptotic behavior of y_1 and y_2 can be found. Since $U \ll V$ for large arguments, only V is retained.

$$y_1 \sim \frac{\pi V}{\Gamma(\Omega^2/2 + 1/2)\, 2^{(1 + \Omega^2)/2}}$$

$$y_2 \sim \frac{\pi V}{\Omega^2 \Gamma(\Omega^2/2)\, 2^{\Omega^2/2}}$$

$$V \sim \pi^{-1/2}\, 2^{\Omega^2 + 1/2}\, H^{\Omega^2} e^{H^2}$$

The use of these and Sterling's formula provide

$$\frac{\varphi}{\varphi_\eta(0)} \sim \frac{\pi^{1/2}\, e^{\Omega\beta}\, 2^{(1 + \Omega^2)/2}}{\Omega^2\, \Gamma(\Omega^2/2)}\, H^{\Omega^2}\, e^{H^2}$$

which with another application of Sterling's formula provides

$$\left(\frac{C}{D}\right)(\Omega R)^{1/2} \sim \exp{-(\Omega^2/2 + \Omega\beta)}\, \Omega^{\Omega^2 + 1}\, 2^{-(\Omega^2 - 1/2)} \tag{A-2}$$

The limiting forms (A-1) and (A-2) are plotted in figure 4.

Appendix B: Edge-layer solutions

Four independent solutions were sought for the edge-layer equation

$$\phi_{0,hhhh} + ie^{-h}(\phi_{0,hh} - \phi_0) = 0 \qquad (B-1)$$

The first three of these, $\phi_0^{(1)}$, $\phi_0^{(2)}$, and $\phi_0^{(3)}$ were obtained by recognizing the series expansions for large positive h.

$$\phi_0^{(1)} \sim 1 + O(e^{-h}) \qquad (B-2)$$

$$\phi_0^{(2)} \sim h + O(he^{-h}) \qquad (B-3)$$

$$\phi_0^{(3)} \sim h^2 + O(h^2 e^{-h}) \qquad (B-4)$$

Then, the function,

$$\phi_0^{(1)} = 1 + ie^{-h} \qquad (B-5)$$

is an exact solution, and

$$\phi_0^{(2)} = h + ie^{-h}(h + 4) + \sum_2^\infty \frac{(-ie^{-h})^k}{(k!)^2 k(k-1)} \qquad (B-6)$$

Kelvin functions in the form

$$J_0 [2(ie^{-h})^{1/2}] = \sum_0^\infty \frac{1}{(k!)^2} (-ie^{-h})^k \tag{B-7}$$

$$\int_0^{e^{-h}} \left\{ 1 - J_0 [2(it)^{1/2}] \right\} \frac{dt}{t} = - \sum_1^\infty \frac{(-ie^{-h})^k}{(k!)^2 k} \tag{B-8}$$

$$(ie^{-h})^{1/2} J_1 [2(ie^{-h})^{1/2}] = - \sum_1^\infty \frac{(-ie^{-h})^k}{[(k-1)!]^2 k} \tag{B-9}$$

are used. From these,

$$\phi_0^{(2)} = h + ie^{-h} (h + 4) + Q_1 [2(ie^{-h})^{1/2}] \tag{B-10}$$

is found, where

$$Q_1(z) = 1 - J_0(z) + 2 \left(1 + \frac{z^2}{4} \right) \int_0^z [1 - J_0(t)] \frac{dt}{t} + \frac{z}{2} J_1(z) \tag{B-11}$$

Similarly, the series representation of $\phi_0^{(3)}$ is

$$\phi_0^{(3)} = h^2 + ie^{-h} (h^2 + 8h + 18) + 2 \sum_2^\infty \frac{(-ie^{-h})^k}{(k!)^2 k (k-1)} \left[(h + 1 + 2\gamma) \right.$$
$$\left. + 2\psi (k+1) + \frac{1}{k} + \frac{1}{k-1} \right] \tag{B-12}$$

where γ is Euler's constant and $\psi(k + 1)$ is the psi (digamma) function. By means of a series manipulation,

$$\sum_{2}^{\infty} \frac{(-iw)^k \psi(k+1)}{(k!)^2 k(k-1)} = \frac{\pi}{2} \left\{ Y_0 \left[2(iw)^{1/2} \right] - (iw)^{1/2} Y_1 \left[2(iw)^{1/2} \right] \right\}$$

$$- \left(\frac{1}{2} \ln w + \frac{i\pi}{4} \right) \left\{ J_0 \left[2(iw)^{1/2} \right] - (iw)^{1/2} J_1 \left[2(iw)^{1/2} \right] \right\}$$

$$- 2(1 + iw) \int_0^{2(iw)^{1/2}} \left\{ -\frac{\pi}{2} Y_0(t) + \left(\ln \frac{t}{2} \right) J_0(t) + \gamma \right\} \frac{dt}{t}$$

$$- \gamma - iw(4 - 3\gamma) - \frac{1}{2} J_0 \left[2(iw)^{1/2} \right] + (iw)^{1/2} J_1 \left[2(iw)^{1/2} \right]$$

$$+ 2iw \int_0^{2(iw)^{1/2}} \left[1 - J_0(t) \right] \frac{dt}{t}$$

(B-13)

$$\sum_{2}^{\infty} \frac{(-iw)^k}{(k!)^2 k(k-1)} \left(\frac{1}{k} + \frac{1}{k-1} \right) = -4iw \int_0^{2(iw)^{1/2}} \left[1 - J_0(t) \right] \frac{dt}{t} + J_0 \left[2(iw)^{1/2} \right] - 1$$

$$- 2(iw)^{1/2} J_1 \left[2(iw)^{1/2} \right] + 2iw + 4(1 + iw) \int_0^{2(iw)^{1/2}}$$

$$\times \int_0^t \left[1 - J_0(s) \right] \frac{ds}{s} \frac{dt}{t}$$

(B-14)

From these equations,

$$\phi_0^{(3)} = h^2 + ie^{-h}(h^2 + 2h) + 2 \left\{ (h + 1 + 2\gamma) Q_1 \left[2(ie^{-h})^{1/2} \right] + Q_2 \left[2(ie^{-h})^{1/2} \right] \right\}$$

(B-15)

59

is found, where

$$Q_2(z) = \pi \left[Y_0(z) - \frac{z}{2} Y_1(z) \right] - 2 \left(\ln \frac{z}{2} \right) \left[J_0(z) - \frac{z}{2} J_1(z) \right] - (1 + 2\gamma)$$

$$- (4 + z^2) \int_0^z \left\{ - \frac{\pi}{2} Y_0(t) + \left(\ln \frac{t}{2} \right) J_0(t) + \gamma - \int_0^t \left[1 - J_0(s) \right] \frac{ds}{s} \right\} \frac{dt}{t} \tag{B-16}$$

Solutions $\varphi_0^{(2)}$ and $\varphi_0^{(3)}$ will be combined and simplified in (B-36) and (B-37).

An attempt to find a fourth series $\varphi_0^{(4)} \sim h^3 + \cdots$ was abandoned in favor of asymptotic representations of φ_0 as $h \to -\infty$. Equation (B-1) should possess two solutions that asymptotically satisfy the "inviscid" limit, where the difference $\varphi_{0,hh} - \varphi_0$ vanishes. Thus, solutions are sought of the form

$$^{(1)}\varphi_0 \sim e^{-h} + \sum_0^\infty a_k e^{hk} \tag{B-17}$$

$$^{(2)}\varphi_0 \sim e^h + \sum_2^\infty b_k e^{hk} \tag{B-18}$$

$^{(1)}\varphi_0$ is simply $-i\varphi_0^{(1)}$, which precludes $^{(1)}\varphi_0$ from being the fourth independent solution desired. Thus $^{(2)}\varphi_0$ is needed. It has the asymptotic expansion

$$^{(2)}\varphi_0 = - 2i \sum_1^\infty \frac{\left[(k - 1)! \right]^2}{k (k + 1)} (ie^h)^k \tag{B-19}$$

60

Because this series was unrecognizable, it was necessary to work with a related function Φ defined by

$$\Phi = w^2 {}^{(2)}\varphi_{0,ww} = -2i \sum_{1}^{\infty} [(k-1)!]^2 \left(\frac{i}{w}\right)^k \qquad (B-20)$$

where w is exp (-h) here and below. Now Φ satisfies the second-order equation

$$w^2 \Phi_{ww} + w\Phi_w + iw\Phi = 2i \qquad (B-21)$$

with complementary solution

$$\Phi_c = AJ_0 [2(iw)^{1/2}] + BH_0^{(1)} [2(iw)^{1/2}] \qquad (B-22)$$

$H_0^{(1)}$ is used rather than Y_0 because it is directly expressible in Kelvin functions:

$$J_0 [2(iw)^{1/2}] = \text{ber} (2w^{1/2}) - i \text{ bei} (2w^{1/2}) \qquad (B-23)$$

$$\frac{\pi i}{2} H_0^{(1)} [2(iw)^{1/2}] = \text{ker} (2w^{1/2}) - i \text{ kei} (2w^{1/2}) \qquad (B-24)$$

A particular solution of (B-21), obtained by the use of an indicial function and Duhamel integration, is

61

$$\Phi_p = -2\pi \left\{ J_0 \left[2(iw)^{1/2}\right] \int^w H_0^{(1)} \left[2(it)^{1/2}\right] \frac{dt}{t} \right.$$

$$\left. - H_0^{(1)} \left[2(iw)^{1/2}\right] \int_\infty^w J_0 \left[2(it)^{1/2}\right] \frac{dt}{t} \right\} \qquad (B-25)$$

By the adjustment of the coefficients A and B of the complementary functions each lower limit in (B-25) is set separately. Most convenient for $H_0^{(1)}$ is ∞. For J_0, any parameter a is chosen. Then, the sum $\Phi_c + \Phi_p$ provides:

$$\Phi = -2\pi \left\{ J_0 \left[2(iw)^{1/2}\right] \int_\infty^w H_0^{(1)} \left[2(it)^{1/2}\right] \frac{dt}{t} \right.$$

$$\left. - H_0^{(1)} \left[2(iw)^{1/2}\right] \left(\int_a^w J_0 \left[2(it)^{1/2}\right] \frac{dt}{t} - FP \int_a^\infty J_0 \left[2(it)^{1/2}\right] \frac{dt}{t} \right) \right\}$$

$$(B-26)$$

where FP denotes the finite part of the integral. Two quadratures then provide the fourth independent solution:

$$^{(2)}\phi_0 = -2\pi \int_\infty^w dw_0 \int_\infty^{w_0} \frac{dw_1}{w_1^2} \left\{ J_0 \left[2(iw)^{1/2}\right] \int_\infty^{w_1} H_0^{(1)} \left[2(iw_2)^{1/2}\right] \frac{dw_2}{w_2} \right.$$

$$- H_0^{(1)} \left[2(iw_1)^{1/2}\right] \left(\int_a^{w_1} J_0 \left[2(iw_2)^{1/2}\right] \frac{dw_2}{w_2} \right.$$

$$\left. \left. - FP \int_a^\infty J_0 \left[2(iw_0)^{1/2}\right] \frac{dw_0}{w_0} \right) \right\}$$

$$(B-27)$$

B.1 Limit $h \to \infty$ (outer edge)

Asymptotic forms for $\phi_0^{(1)}$, $\phi_0^{(2)}$, and $\phi_0^{(3)}$ are shown in (B-2), (B-3), and (B-4). Use of the expansions

$$\int_\infty^w H_0^{(1)} [2(it)^{1/2}] \frac{dt}{t} \sim \frac{i}{2\pi} (\ln w)^2 + \left(\frac{1}{2} + i \frac{2\gamma}{\pi}\right) \ln w$$

$$- FP \int_0^\infty H_0^{(1)} [2(it)^{1/2}] \frac{dt}{t} + O(w \ln w)$$

$$\tag{B-28}$$

$$\int_a^w J_0 [2(it)^{1/2}] \frac{dt}{t} \sim \ln w - FP \int_0^a J_0 [2(it)^{1/2}] \frac{dt}{t} + O(w) \tag{B-29}$$

results in the following representation for Φ:

$$\Phi \sim ih^2 + 2ih \, dfp + \left[2\pi \, FP \int_0^\infty H_0^{(1)} [2(it)^{1/2}] \frac{dt}{t} - (\pi + i4\gamma) \, dfp \right] + TST$$

$$\tag{B-30}$$

where

$$dfp \equiv FP \int_0^a J_0 [2(it)^{1/2}] \frac{dt}{t} + FP \int_a^\infty J_0 [2(it)^{1/2}] \frac{dt}{t} \tag{B-31}$$

The two quadratures of Φ/w^2 then result in the asymptotic form desired, i.e.,

$$^{(2)}\phi_0 \sim \left(\frac{i}{3}\right) h^3 + e_2 h^2 + e_1 h + e_0 \tag{B-32}$$

63

where

$$e_2 = -i\left[1 - dfp\right] \tag{B-33}$$

$$e_1 = 2i\left[1 - dfp\right] + 2\pi\,FP\int_0^\infty H_0^{(1)}\left[2(it)^{1/2}\right]\frac{dt}{t} - (\pi + i4\gamma)\,dfp \tag{B-34}$$

$$e_0 = FP\,{}^{(2)}\phi_0 = FP\int_{-\infty}^0 e^{-h_1}\int_\infty^{h_1} e^{h_2}\,\Phi(h_2)\,dh_2 dh_1 \tag{B-35}$$

Although all three e_i can be evaluated, they have not been, because they are not needed for zero-order matching. The coefficient $i/3$ of the cubic term in (B-32) is needed, which justifies obtaining ${}^{(2)}\phi_0$ and its limiting form shown.

B.2   Limit $h \rightarrow -\infty$ (inner edge)

From (B-5) it is clear that as $h \rightarrow -\infty$, $\phi_0^{(1)} \sim i \exp(-h)$, and, from (B-18) that ${}^{(2)}\phi_0 \sim \exp(h)$. Examination of (B-11) indicates that $\phi_0^{(2)}$ grows as $h \rightarrow -\infty$ much more rapidly than $\exp(-h)$.

The same is true for $\phi_0^{(3)}$. There is, however, a linear combination of $\phi_0^{(2)}$ and $\phi_0^{(3)}$ for which this rapid variation cancels. That combination is

$$f = \phi_0^{(3)} + (\pi i - 2 - 4\gamma)\,\phi_0^{(2)} \tag{B-36}$$

64

If $x = 2e^{-h/2}$, f can be written as

$$f(x) = (4 + ix^2) \left[\ln\left(\frac{x}{2}\right)\right]^2 + \ln\left(\frac{x}{2}\right) \left[4 - (4 + ix^2) \frac{(\pi i - 4\gamma)}{2}\right]$$

$$- \left(\frac{x^2}{4}\right) (\pi + 2i + 4\gamma i) - \left(4 + 2x \frac{d}{dx} [kr(x) - i\,ki(x)]\right)$$

$$- 2 (4 + ix^2) \int_0^x t^{-1} [kr(t) - i\,ki(t)]\, dt \qquad (B-37)$$

where

$$kr(x) - i\,ki(x) \equiv \left(\frac{\pi i}{2}\right) H_0^{(1)} (xe^{i\pi 4}) + \ln\left(\frac{x}{2}\right) + \gamma - i\pi/4$$

The integral in (B-37) vanishes as $x \to 0$, since $kr(x) - i\,ki(x)$ is of order $x^2 \ln x$. Equation (B-37) does not contain any of the $J_0 (xe^{i\pi 4})$ terms that caused $\phi_0^{(2)}$ and $\phi_0^{(3)}$ to become unbounded for large x. Since $H_0^{(1)} (xe^{i\pi 4})$ vanishes for large x (the inner edge), an asymptote for f that is merely exponental in $|h|$ is left.

$$f \sim \phi_0^{(1)} (c_r + i c_i) + o(e^h) \qquad (B-38)$$

where

$$c_r = -8 \int_0^1 t^{-1} [ker(t) + \ln(t/2) + \gamma]\, dt - 8 \int_1^\infty t^{-1} ker(t)\, dt$$

$$-4\gamma (2 \ln 2 + 1) - 2 + 4 (\ln 2)^2 \qquad (B-39)$$

65

$$c_i = 8 \int_0^1 t^{-1} \left[kei\,(t) + \frac{\pi}{4} \right] dt + 8 \int_1^\infty t^{-1} kei\,(t)\,dt + \pi\,(2\,\ln 2 + 1)$$

(B-40)

Numerically, c_r and c_i are -6.46404 and 6.76836, respectively.

REFERENCES

Abramowitz, M. and Stegun, I. A. eds. 1966. Handbook of Mathematical Functions, Applied Mathematics Series 55, National Bureau of Standards, Washington, D. C., Chapt. 9 and 19.

Antar, B. N. and Benek, J. A. 1978. Temporal eigenvalue spectrum of the Orr-Sommerfeld equation for the Blasius boundary layer, Phys. of Fluids, 21, 183.

Arnal, D. and Juillen, J.-C. 1977. Experimental and theoretical study of boundary layer transition, Recherche Aerospatiale 2, 75-88.

Criminale, W. O. 1971. On structure of the laminar boundary layer in the presence of a fluctuating freestream, Intern. Union Theoretical and Applied Mechanics Symposium on Unsteady Boundary Layers, Quebec, Canada.

Criminale, W. O. 1976. Interaction of the laminar boundary layer with free-stream turbulence, Phys. of Fluids, 10, 101-107.

Goldstein, S. 1956. Flow of an incompressible viscous fluid along a semi-infinite flat plate, HE-150-144, Engineering Research Institute, University of California, Los Angeles, California.

Goldstein, S. 1960. Lectures on Fluid Mechanics, New York: Wiley Interscience.

Graebel, W. P. 1966. On determination of the characteristic equations for the stability of parallel flows, J. Fluid Mech. 24, 497-508.

67

Grosch, C. E. and Salwen, H. 1978. The continuous spectrum of the
Orr-Sommerfeld equation, J. Fluid Mech, 87, 33.

Illingworth, C. R. 1958. The effects of a sound wave on the compressible
boundary layer on a flat plate, J. Fluid Mech. 3, 471-493.

Imai, I. 1957. Second approximation to the laminar boundary layer flow
over a flat plate, J. Aeronaut. Sci. 24, 155-156.

Jordinson, R. 1971. Spectrum of eigenvalues of the Orr-Sommerfeld
equation for Blasius flow, Phys. of Fluids, 14, 2535-2537.

Kachanov, Y. S., Kozlov, V. V., and Levchenko, V. Y. 1976. Physical
gas dynamics, in Aerophysical Research, Vol. 6, Institute of
Theoretical and Applied Mechanics, Siberia AN SSR, Novosibirsk.

Kestin, J., Maeder, P. F. and Wang, H. E. 1961. On boundary layers
associated with oscillating streams, Appl. Sci. Res. 10, 1-22.

Mack, L. M. 1975. Linear stability theory and the problem of supersonic
boundary layer transition, AIAA 13, 278-289.

Mack, L. M. 1976. A numerical study of the temporal eigenvalue spectrum
of the Blasius boundary layer. J. Fluid Mech., 73, 497-520.

Mack, L. M. 1977. Transition and Laminar Instability, Jet Propulsion
Laboratory, Pasadena, California, Report No. 77-15, p. 45; also,
1978 Application and Fundamentals of Turbulence, New York: Plenum
Press, Chapt. 3.

Murdock, J. W. and Stewartson, K. 1977. Spectra of the Orr-Sommerfeld
equation, Phys. of Fluids, 28, 1404-1411.

Patel, M. H. 1975. On laminar boundary layers in oscillatory flows, *Proc. Royal Soc. London, Series A* 347, 99-123.

Reshotko, E. 1976. Boundary layer stability and transition, in *Annual Review of Fluid Mechanics*, Vol. 8, Annual Reviews, Inc., Palo Alto, California, p. 330 and 344.

Riley, N. 1975. Unsteady laminar boundary layers, *SIAM Rev.* 17, 274-297.

Rogler, H. L. and Reshotko, E. 1975. Disturbances in a boundary layer introduced by a low intensity array of vortices, *SIAM J. Appl. Math.*, 28, 431-462.

Ross, J. A., Barnes, F. H., Burns, J. G., and Ross, M. A. S. 1970. The flat-plate boundary layer, Part 3: Comparison of theory with experiment, *J. Fluid Mech.* 43, 819-832.

Rott, N. 1964. Theory of time-dependent laminar flows, in *Theory of Laminar Flows*, Vol. IV: *High Speed Aerodynamics and Jet Propulsion*, Princeton, New Jersey: Princeton University Press, p. 407.

Schubauer, G. B. and Skramstad, H. K. 1948. *Laminar Boundary Layer Oscillations and Transition on a Flat Plate*, N.A.C.A. Report No. 909 NASA, Washington, D.C.

LABORATORY OPERATIONS

The Laboratory Operations of The Aerospace Corporation is conducting experimental and theoretical investigations necessary for the evaluation and application of scientific advances to new military concepts and systems. Versatility and flexibility have been developed to a high degree by the laboratory personnel in dealing with the many problems encountered in the nation's rapidly developing space and missile systems. Expertise in the latest scientific developments is vital to the accomplishment of tasks related to these problems. The laboratories that contribute to this research are:

Aerophysics Laboratory: Launch and reentry aerodynamics, heat transfer, reentry physics, chemical kinetics, structural mechanics, flight dynamics, atmospheric pollution, and high-power gas lasers.

Chemistry and Physics Laboratory: Atmospheric reactions and atmospheric optics, chemical reactions in polluted atmospheres, chemical reactions of excited species in rocket plumes, chemical thermodynamics, plasma and laser-induced reactions, laser chemistry, propulsion chemistry, space vacuum and radiation effects on materials, lubrication and surface phenomena, photosensitive materials and sensors, high precision laser ranging, and the application of physics and chemistry to problems of law enforcement and biomedicine.

Electronics Research Laboratory: Electromagnetic theory, devices, and propagation phenomena, including plasma electromagnetics; quantum electronics, lasers, and electro-optics; communication sciences, applied electronics, semiconducting, superconducting, and crystal device physics, optical and acoustical imaging; atmospheric pollution; millimeter wave and far-infrared technology.

Materials Sciences Laboratory: Development of new materials; metal matrix composites and new forms of carbon; test and evaluation of graphite and ceramics in reentry; spacecraft materials and electronic components in nuclear weapons environment; application of fracture mechanics to stress corrosion and fatigue-induced fractures in structural metals.

Space Sciences Laboratory: Atmospheric and ionospheric physics, radiation from the atmosphere, density and composition of the atmosphere, aurorae and airglow; magnetospheric physics, cosmic rays, generation and propagation of plasma waves in the magnetosphere; solar physics, studies of solar magnetic fields; space astronomy, x-ray astronomy; the effects of nuclear explosions, magnetic storms, and solar activity on the earth's atmosphere, ionosphere, and magnetosphere; the effects of optical, electromagnetic, and particulate radiations in space on space systems.

THE AEROSPACE CORPORATION
El Segundo, California